Physics – Uspekhi **66** (1) 32 – 58 (2023)

REVIEWS OF TOPICAL PROBLEMS PACS numbers: 05.70.Ce, 05.70.Ln, 62.20.M –

Physics of severe plastic deformation

A M Glezer, R V Sundeev, A V Shalimova, L S Metlov

DOI: https://doi.org/10.3367/UFNe.2021.07.039024

Contents

Abstract. The review describes a number of important recent studies in the field of physical fundamentals of severe plastic deformations (SPDs) in metals and alloys and their further systematization. Based on analyses of experimental data and theoretical approaches, we formulate for the first time three fundamental principles and seven characteristic features inherent in SPD processes. SPD physics is entirely based on the postulates of nonequilibrium thermodynamics. A solid under deformation is considered a mechanical dissipative system in which the total energy continuously decreases or dissipates, converting into other, nonmechanical, forms of energy. Within the framework of the proposed nonequilibrium evolutionary thermodynamics, it is possible to describe from a unified standpoint the evolution of the structure of defects for polycrystalline and amorphous metallic materials upon SPD. We note that the process of mechanical alloying of powders should not be completely identified with SPD processes.

A M Glezer[(1,2)], **R V Sundeev**[(3,a)], **A V Shalimova**[(2,b)], **L S Metlov**[(4,5,c)]

[(1)] National University of Science and Technology MISIS, Leninskii prosp. 4, 119049 Moscow, Russian Federation

[(2)] Bardin Research Institute for Ferrous Metallurgy; ul. Radio 23/9, str. 2, 105005 Moscow, Russian Federation

[(3)] MIREA — Russian Technological University, prosp. Vernadskogo 78, 119454 Moscow, Russian Federation

[(4)] Galkin Physical-Technical Institute, ul. R. Luksemburg 72, Donetsk, Russian Federation

[(5)] Donetsk National University, ul. Universitetskaya 24, Donetsk, Russian Federation

E-mail: [(a)] sundeev55@yandex.ru, [(b)] shalimanna@yandex.ru, [(c)] lsmet@donfti.ru

Received 3 July 2021
Uspekhi Fizicheskikh Nauk **193** (1) 33 – 62 (2023)
Translated by V L Derbov

Keywords: severe plastic deformation, structures, fragmentation, dynamic recrystallization, nonequilibrium thermodynamics, defects, dissipation, internal energy, diffusion, phase transformations, amorphous state, evolution equations

Dedicated
to the blessed memory
of the outstanding Russian physicist
Vladimir Evgen'evich Fortov

1. Introduction

Extreme external actions substantially affect the structure and properties of solids [1–6]. Undoubtedly, the effect of severe plastic deformations should be considered one of them. In recent years, interest in this method of affecting materials has significantly increased, since it promises to allow creating special nanostructured states and thereby significantly improving the physical and mechanical properties of metallic materials [7]. The authors of Ref. [8] even suggested that the impact by severe plastic deformations opens up interesting opportunities for the synthesis of new materials, in which new promising structural models can be implemented, borrowed from a rich palette of patterns found in inanimate nature, especially in Earth's lithosphere.

Since the classical dislocation and disclination approaches, successfully used earlier to describe ordinary macroscopic deformations, turned out to be insufficient in this case, in recent years a number of important fundamental and applied studies have appeared that allow clarifying to a certain extent the physical picture of the structural processes inherent in severe plastic deformations. This review is devoted to a generalized analysis of these studies.

The study of the physics of severe plastic deformations undoubtedly began with the work of the Nobel Prize winner P W Bridgman. For many years, he experimentally studied severe plastic deformations and destruction in solids, both

crystalline (metals and alloys) and amorphous (plastics and boric anhydride B_2O_3), under high hydrostatic pressure during tensile, compression, torsion, shear, and other stresses [9–16]. Using the original setups designed by him, new phenomena occurring at severe deformations were discovered for the first time. It is impossible not to admire Bridgman's bold hypothesis: "*It is conceivable that the crystal might be broken up into a mosaic of smaller and smaller blocks, with little alteration of structure within the block...*" ([9], p. 286). In fact, Bridgman predicted the unique phenomenon of fragmentation, which, as it turned out later, plays a fundamental role upon severe deformations. Based on his experiments, he also predicted the possibility of the transition of a material under severe deformation from a crystalline state to an amorphous state: "*It was found, for example, that under intense shearing the crystal structure of copper is so far broken down that only a single very diffuse characteristic X-ray line can be detected, meaning a grain size probably less than* 10 Å *on a side*" ([9], p. 287). Although Bridgman used setups with various schemes for creating a stress state, today only the Bridgman chamber is used productively, in which, at a high quasi-hydrostatic pressure (several GPa), a large torsional deformation of a sample clamped between two anvils is realized by rotating a movable anvil relative to a stationary one. This technique is known as high-pressure torsion (HPT) [17].

In our country, the effect of hydrostatic pressure on the physical and mechanical properties of materials began to be studied under the leadership of Academicians L F Vereshchagin [18] and N S Enikolopyan [19]. Further impetus in the investigation of severe plastic deformations is associated with studies by V M Segal [20] and R Z Valiev [21], who proposed to implement severe deformations by means of the equal channel angular pressing (ECAP) method. Later, twist extrusion, accumulative rolling, free forging, and other methods have been used to obtain special structural states under severe plastic deformations [20]. The plastic deformations realized in this case are so significant that the common relative degrees of deformation lose their meaning, and one should use true logarithmic strain e.

While the boundary separating microplastic and macroplastic strain is clearly defined by the degree of deformation corresponding to the macroscopic yield strength (relative strain $\varepsilon = 0.05$ or 0.2%), the boundary between macroplastic strain and severe plastic strain remains indefinite. Conventionally, we will consider the boundary to be the relative deformation $\varepsilon \approx 100\%$ (true strain $e \approx 1$). Below, we will try to determine a more rigorous, physically substantiated value of plastic deformation corresponding to such a transition.

2. Specific features of severe plastic deformations

Summarizing a large number of experimental studies of the structure and properties of materials subjected to severe plastic deformations, we can distinguish the following seven characteristic phenomena observed in this case [7]:

(1) Fragmentation. Formation of a high volume density of high-angle boundaries and, accordingly, the formation of almost defect-free deformation fragments.

(2) Absence of the strain hardening stage on the plastic strain curves.

(3) Processes of low-temperature dynamic recrystallization.

(4) Abnormally high diffusive mobility of atoms.

(5) Cyclic nature of structural phase transformations.

(6) Phase transformations accompanied by segregation of nonequilibrium phases and/or dissolution of equilibrium phases depending on the temperature and deformation conditions.

(7) Processes of crystalline phase amorphization and amorphous state crystallization.

3. Basic concepts of severe plastic deformations

There is no coherent theory of structure formation under severe plastic deformations in the literature which is capable of explaining all the above features of the late stages of plastic deformation from a unified physical standpoint. We consider here the most productive, in our opinion, physical approach based on the following three fundamental principles [22, 23]:

I. Severe plastic deformation is a structurally determined, independent, and specific stage of plastic deformation inherent in all solids and proceeding under certain conditions in all stress state systems according to special mechanisms, including dislocation, disclination, and other structural modes of active plastic flow and structural rearrangements having a relaxation and dissipative nature.

II. The mechanical energy introduced in severe plastic deformations is so great that one should consider a deformable solid in the framework of nonequilibrium thermodynamics as a mechanical dissipative system (MDS), in which the total energy is continuously reduced or dissipated, converting into other, nonmechanical forms of energy (chemical, electromagnetic, thermal, etc.).

Much later, a similar approach based on nonequilibrium thermodynamics was proposed in [24] under the nonobvious assumption that diffusion processes play a dominant role in severe plastic deformations.

III. Structural processes that occur during severe plastic deformations can be divided into two independent (or weakly coupled) groups: processes directly responsible for the implementation of plastic flow and accompanying processes that affect plastic deformation only indirectly. The first group should include the formation of all possible defects of a deformation origin (dislocations, disclinations, shear bands, grain boundaries, and deformation fragments), and the second group, the formation of concentration inhomogeneities of a diffusive origin and nonequilibrium (crystalline, ordered, and amorphous) phases. The first group of processes, as a rule, is due to athermal atomic rearrangement mechanisms, and the second group is a result of thermally activated processes (except martensitic-type phase transformations).

Following the first principle of implementing severe plastic deformations, it is necessary to consider three separate, although physically interconnected, stages of plastic flow evolution (Fig. 1). The first (initial) stage is known as the process of *microplastic deformation* [25]. It

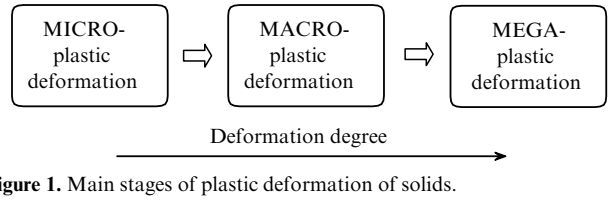

Figure 1. Main stages of plastic deformation of solids.

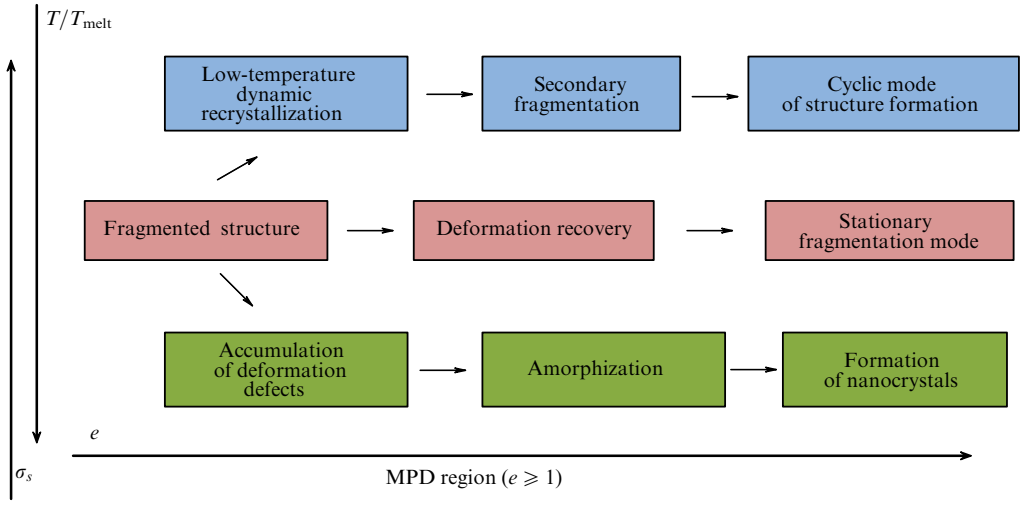

Figure 2. Basic scenarios ('road map') of the development of structural transformations in the process of MPD of a single-phase material; T/T_{melt} is the ratio of deformation and melting temperature, respectively; σ_s is the Peierls barrier; e is the true deformation.

proceeds until the deforming stress reaches the value of the macroscopic yield strength. The second stage is known as *macroplastic deformation*, which occurs under deforming stresses above the yield point [26]. The characteristic features of both of these deformation stages have been studied in detail. At the first stage, deformation processes are localized within individual crystal grains, have clear morphological signs (Chernov–Luders bands), and are characterized by inelasticity effects [27]. At the second stage, the processes of dislocation flow and/or mechanical twinning cover the entire polycrystalline ensemble of grains and are characterized mainly by the nucleation, elastic interaction, and annihilation of dislocations under the conditions of manifestation of strain hardening effects [26]. The third independent stage in Fig. 1 corresponds to severe plastic deformations and includes the manifestation of at least one of the specific signs of severe deformation mentioned in Section 2.

As is known [28], there are three scale levels of the material world: the *microworld* — the scale of individual atoms and molecules, the *macroworld* — the scale of human perception of the world (meter, kilogram, second), and the *megaworld* — the astronomical scale. By analogy, the stage of severe plastic deformations should be called *megaplastic* deformation (MPD), which corresponds to the general logic of the development of any material phenomenon.

The MPD process has a fundamentally nonequilibrium character, and it is appropriate to apply the principles of nonequilibrium evolutionary thermodynamics (NET) to describe its kinetics [29]. Within NET, it is possible to describe almost all the characteristic MPD phenomena mentioned in Section 2. In Ref. [30], a thermodynamic identity combining the first and second laws of thermodynamics (the Gibbs equality) was proposed for a particular case of MPD simulation in polycrystalline metals and alloys.

The internal processes occurring in a solid represent a complex picture of mutual transitions and transformations of energy [31], and they can be considered as part of the general relaxation process [32]. Acting mechanically on a finite-size solid body, we 'pump' a certain energy into it. The obvious channel of elastic energy relaxation is plastic deformation. When it is exhausted, an alternative channel may turn on, namely, mechanical destruction. However, at significant elastic energy values, plastic deformation can initiate, in principle, additional channels of relaxation: dynamic recrystallization, phase transformations, and additional release (dissipation) of heat. In the case of MPD, when, as a rule, the component of all-around compression stresses is large, the formation and growth of splitting cracks is partially or completely suppressed, and, therefore, fracture is significantly more difficult. Using schemes with a large component of compressive stresses (1D, 2D, or 3D), we 'force' a solid body to deform without breaking, and thereby to proceed from the macroscopic strain to MPD, in which an active role is played by qualitatively new relaxation processes of low-temperature dynamic recrystallization, phase transformations, including the formation of nonequilibrium phases and structure amorphization, and/or heat release [33].

The authors of Ref. [34] proposed three possible scenarios (a 'road map') for the development of further events in pure metals and single-phase compounds within the framework of MDSs (Fig. 2). When the processes of dislocation and disclination rearrangements are facilitated in a material (e.g., in pure metals), after the stage of developed deformation (fragmentation) is completed, low-temperature dynamic recrystallization occurs (upper branch in Fig. 2). The local regions of the structure are 'cleared' of defects, and the process of plastic flow begins again in new recrystallized grains through dislocation and disclination modes. In this case, dynamic recrystallization acts as a powerful additional channel for the relaxation of elastic energy, and the stages of fragmentation and dynamic recrystallization cyclically alternate as deformation increases in given areas of the solid. When the mobility of plastic deformation carriers is relatively low (e.g., at cryogenic temperatures), phase transitions serve as a powerful additional channel for the relaxation of mechanical energy (lower branch in Fig. 2). Most often, this is a 'crystal → amorphous state' transformation. As a result, the plastic flow is localized in the amorphous matrix without the effects of strain hardening or the accumulation of large internal stresses. There is an intermediate case (middle branch in Fig. 2) when effective dislocation-disclination accommodation processes can serve as an additional relaxation channel, which leads to the stabilization of the fragmented structure observed in some experiments as the MPD develops. Switch-

ing from one scenario of structural rearrangements to another depends on the parameter $T_{\mathrm{MPD}}/T_{\mathrm{melt}}$ for the selected material, where T_{MPD} is the MPD temperature allowing for possible heat release, and T_{melt} is the melting point.

4. Nonequilibrium evolutionary thermodynamics

Since the density of structural defects increases by orders of magnitude during MPD, the plastic deformation process is fundamentally nonequilibrium in nature, and it is reasonable to describe its kinetics using the principles of nonequilibrium evolutionary thermodynamics [29]. In this model, it is possible to describe the main features of the defect structure formation in polycrystalline metals during treatment by SPD methods [20, 32, 35].

The internal processes occurring in a solid represent a complex picture of mutual transitions and transformations of energy [36]. The dissipation of energy with the participation of defects is dynamic in nature and is accompanied by transient phenomena such as acoustic emission. The kinetic energy that arises in defect formation is first radiated in the form of low-frequency waves [32], which can be considered a part of the general relaxation process. The scattering of these waves by equilibrium thermal vibrations completes the relaxation process with the participation of defects. Thus, energy takes the equilibrium thermal form after passing through a series of intermediate stages rather than immediately.

In the case of irreversible processes, part of the work of external forces goes into internal heating, and the work of external forces can be divided into reversible and irreversible parts [29]:

$$\mathrm{d}u = \sigma_{ij}\,\mathrm{d}\varepsilon_{ij}^{\mathrm{e}} + \sigma_{ij}\,\delta\varepsilon_{ij}^{\mathrm{n}} + T\,\delta s'\,, \tag{1}$$

where u is the internal energy density; σ_{ij} and ε_{ij} are the stress tensor and the strain tensor; T is the temperature; s' is the density of entropy from external sources; and $\varepsilon_{ij}^{\mathrm{e}}$ and $\varepsilon_{ij}^{\mathrm{n}}$ are the elastic and inelastic strains.

The irreversible part of the work of external stresses (the second term in Eqn (1)) is spent for the formation of objects with excess potential energy (phonons, micropores, grain boundaries, etc.), which determine the energy dissipation channels. Summing up the production of entropy from external and internal sources, we arrive at the thermodynamic Gibbs identity combining the first and second laws of thermodynamics [30]:

$$\mathrm{d}u = \sigma_{ij}\,\mathrm{d}\varepsilon_{ij}^{\mathrm{e}} + T\,\delta s' + T\,\delta s'' = \sigma_{ij}\,\mathrm{d}\varepsilon_{ij}^{\mathrm{e}} + T\,\mathrm{d}s\,. \tag{2}$$

Here, the additional heat generated by internal sources is assumed to have already come to the equilibrium state; therefore, the same equilibrium temperature is used for both thermal contributions. Note that the equilibrium definition of temperature is used to describe strongly nonequilibrium processes. The reason is that a high degree of nonequilibrium is associated here with structural changes, and purely thermal processes are assumed to be either equilibrium or weakly nonequilibrium from the point of view of the standard concept of a locally equilibrium state.

Nonequilibrium heat can be present in the system either as thermal fluctuations or as the generation of nonequilibrium phonons due to the creation and motion of defects. In the first case, this quantity is small and can be disregarded for large systems. In the second case, it is present as an intermediate product of relaxation. Because of the formation and migration of defects under intense external action, it is generated all the time uniformly throughout the entire volume, but, due to nonlinear scattering by equilibrium thermal phonons and lattice inhomogeneities, their energy is constantly redistributed to the equilibrium thermal subsystem [17].

If work is irreversibly spent not only for heating but also for creating high-energy structural defects in the volume of a solid (e.g., additional interfaces or dislocations during MPD), then we have [25]

$$\sigma_{ij}\,\delta\varepsilon_{ij}^{\mathrm{n}} = T\,\delta s'' + \varphi_m\,\delta h_m\,, \tag{3}$$

where the mean energy φ_m and the volume density h_m of m-type defects form a conjugate pair of thermodynamic variables, which characterize the material defectiveness. The index m takes the values $1, 2, \ldots, M$, where M is the number of types of structural defects created in the course of MPD. Relation (3) can be considered a law of energy transformation or conservation for internal degrees of freedom in elementary events with all main dissipation channels taken into account.

The final thermodynamic identity without taking into account the nonequilibrium heat $T^*\delta s^*$ has the form [29]

$$\mathrm{d}u = \sigma_{ij}\,\mathrm{d}\varepsilon_{ij}^{\mathrm{e}} + T\,\mathrm{d}s + \varphi_m\,\mathrm{d}h_m\,. \tag{4}$$

Equation (4) expresses the combined (first and second) law of thermodynamics in the form of equality (the generalized Gibbs relation). In the general case, it is a kind of approximation, since it takes into account only some of the main dissipation channels rather than all possible ones. With the right choice of the main channels of dissipation, the relations can be quite accurate.

The increments of independent thermodynamic variables $\varepsilon_{ij}^{\mathrm{e}}$, s, and h_m in Eqn (4) are total differentials. Therefore, the internal energy is a function of these variables and, in the considered approximation, they completely determine the state of the system. Conjugate to them, dual variables σ_{ij}, T, and φ_m are calculated by simple differentiation of the internal energy.

The variable φ_m can be interpreted as nonequilibrium energy (or nonequilibrium chemical potential) of an m-type defect, which take both positive and negative values, but in stationary states must be only a positive (observable) quantity. If the current state does not coincide with the stationary state, then the transition to the stationary state can be described by Landau–Khalatnikov equations, but in terms of the internal energy:

$$\frac{\partial h_m}{\partial t} = \gamma_m\left(\frac{\partial u}{\partial h_m} - \varphi_{m\mathrm{s}}\right) = \gamma_m(\varphi_m - \varphi_{m\mathrm{s}})\,. \tag{5}$$

Here, the derivatives of the internal energy with respect to nonequilibrium variables are the generalized thermodynamic forces, γ_m are the kinetic coefficients, and $\varphi_{m\mathrm{s}}$ is the defect energy in the stationary state. With the appropriate techniques available, it can be measured experimentally.

5. Structural models of specific effects during severe plastic deformation

Below, we consider the most significant structural models that have been proposed so far to describe the specific features of MPD mentioned in Section 2. Note that all of them, with rare exceptions, were formulated at the time for the sole

purpose of correctly describing the phenomenon of fragmentation of initial crystals with the formation of strongly disoriented deformation small-size fragments.

5.1 Fragmentation

The key task of a theoretical description of the processes occurring during MPD is to explain the effect of fragmentation — a decrease in the average size of grains (fragments) as MPD evolves and reaches saturation at a grain size of about 0.1–0.2 μm.

The essence of the proposed approach within the framework of plastic flow mechanics is to consider monotonic and nonmonotonic plastic flow processes differently affecting the microstructure and physical and mechanical properties of materials [38, 39]. In monotonic processes, the components of the stress deviator increase monotonically in proportion to one parameter, while the principal axes of the stress tensors and strain rate tensors always coincide with the same principal geometric axes of the material. Examples of such processes are uniaxial tension and compression, and longitudinal rolling and drawing. According to the authors of the above-mentioned papers [38, 39], as well as some other authors, after monotonic deformation, a weakly disoriented cellular substructure and deformation microbands are formed in materials. As a result of nonmonotonic deformation, highly disoriented nanograins are formed in metals, which ensures their high mechanical and functional qualities. Based on the laws of plastic deformation mechanics, the difference between the formed microstructures is determined by different scalar and vector characteristics of monotonic and nonmonotonic deformations. In the first case, a monotonic accumulation of deformation occurs in the material, and in the second case, severe deformations accumulate and rotational modes are realized, as a result of which shear bands appear, followed by the formation of small (0.1–0.2 μm) fragments separated by high-angle boundaries [38]. In the case of nonmonotonic processes, the main axes of the strain tensors are assumed to rotate through large angles relative to their own coordinate system due to the effect of the rotational strain component [40, 41]. These processes include ECAP, HPT, and twist extrusion.

Significant nonmonotonicity of the load is characterized by a large curvature or bending of the loading paths. A particular case of complex loading is a simple shear with a large equivalent strain [42], which is assumed to be the main mechanical method of deformation in the above-mentioned MPD processes. According to supporters of this concept, the main feature in the formation of the microstructure of metallic materials, which determines simple shear, is that, in contrast to pure shear, it leads to the early formation of shear bands and their further transformation into deformation fragments [43].

The authors of Ref. [38] propose that the processes of monotonic deformation, in which no fragmentation effects are observed, be called 'large plastic deformations,' and the processes of nonmonotonic deformation leading to deformation fragmentation be called 'intense plastic deformations.' In doing so, they not only do not clarify the overall picture, but even more complicate the understanding of the physical processes occurring under significant deformations and create considerable confusion. First, the term 'large plastic deformation' was already used by Bridgman to describe the processes leading to the deformation fragmentation he discovered [44]. Second, the hypothesis of [38] that the effects of deformation fragmentation can be realized only under certain schemes of the stress state under conditions of nonmonotonic deformation and simple shear is erroneous in principle. Fragments separated by high-angle boundaries have been repeatedly observed during rolling and other types of monotonic deformations in numerous studies (in particular, by P W Bridgman [9, 44] in compression and by V V Rybin [45] in rolling), thus demonstrating the unacceptability of the above approach within the framework of plastic deformation mechanics.

Reviews [46, 47] consider in detail analytical and numerical approaches to modeling structural rearrangements during MPD exclusively in the framework of dislocation concepts. Special attention is paid to the significant influence of heat release and dynamic recrystallization processes. However, it turns out to be impossible to achieve a complete and unambiguous description of the features of the mechanical behavior of materials in the process of MPD solely within dislocation concepts.

V V Rybin [45] and his followers [48] proposed the most physically correct and harmonious concept of the fragmentation nature in MPD. Based on the idea of the dominant role of the disclination mode in the implementation of MPD and related fragmentation processes, they managed to describe correctly the phenomena that occur at significant degrees of deformation close to $e = 1$. Figure 3 shows an electron microscopic image of a disclination dipole at the stage of the fragmented structure formation during cold rolling of molybdenum. In accordance with the disclination concept, the size of the fragments — the main structural elements — gradually decreases with increasing deformation, reaching a minimum value of about 0.2 μm, after which it remains constant. The stage of active fragmentation was defined as *developed plastic deformation*. In fact, this means that the transition to the region of a nanostructural state with a fragment (grain) size of less than 100 nm (0.1 μm) under the action of the disclination mode at the stage of developed deformation is hardly possible. Analysis of numerous experimental data, especially for bcc crystals, led V V Rybin to the concept of a limiting (critical) fragmented structure, whose further evolution within the disclination mode becomes impossible [45]. The centers of destruction are formed along the boundaries of the fragments separating the regions, as a rule, free from dislocations. The critical fragmented structure, in the opinion of the author of Ref. [45], is the final product of plastic deformation; it is not able to resist the increasing

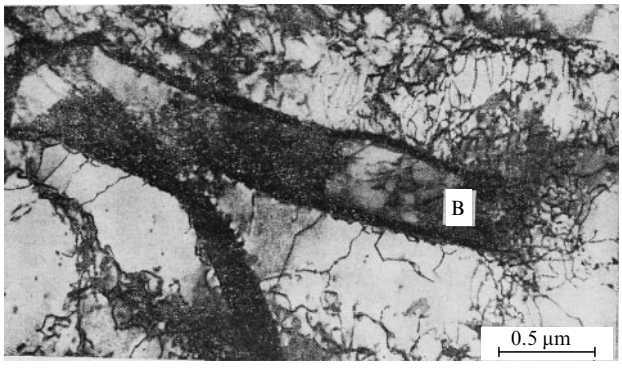

Figure 3. Dipole configuration (B) consisting of two broken tilt boundaries in molybdenum deformed by rolling at the stage of developed plastic deformation. (Transmission electron microscopy [45].)

influence of external and internal stresses and must lead to destruction. The above critical fragmented structures were formed at $e \leqslant 2$ for the case of uniaxial tension or rolling of bcc metals. The question arises: how is it possible to achieve much more significant deformations in the course of numerous experiments at the stage of MPD? Unfortunately, the theory of developed plastic deformation does not answer the question of why the stage of MPD occurs after it. Another 'mismatch' between Rybin's model and experiment is that, according to his theory, the maximum on the distribution curve of deformation fragments over disorientation angles should gradually shift towards larger values as the MPD increases. In fact, as the strain increases, a second maximum appears on the distribution curve, corresponding to a disorientation angle of about 60° between fragments [49]. This, apparently, indicates the existence of an alternative fragmentation mechanism associated with the occurrence of continuous dynamic recrystallization processes [50].

Another explanation for fragmentation was proposed in Refs [51, 52]. According to their theoretical concepts, various kinds of dislocation- and disclination-type defects accumulate at the grain boundaries during MPD, giving rise to powerful stresses inside the grain. The latter induce the creation of collective modes of dislocation motion in the form of broken boundaries, which, becoming entangled in the process of motion, lead to grain refinement. The fragmentation condition is formulated as a requirement that the intensity of the internal stress fields created by junction disclinations in grains σ_i be higher than the plastic limit σ_1, i.e., $\sigma_i \geqslant \sigma_1$. For that, the power of junction disclinations must be above a certain limit, $\omega \geqslant \omega^*$. When grains are refined, the mechanism of accommodation by generating broken boundaries becomes replaced with the fast diffusion mechanism. Within the framework of the proposed approach, the hypothesis that 'special' nonequilibrium grain boundaries are formed as a result of MPD became extremely widespread [53]. These boundaries, in the opinion of some authors, are responsible for the anomalous phenomena of slip, diffusion, and interaction with lattice defects, and, as a result, may be responsible for high values of strength and plasticity.

Also known is the theory of fragmentation of dislocation structures based on the concepts of self-organization of dislocations [54]. Bending and torsional stresses and strains that occur during ECAP lead to the generation of a large number of geometrically necessary dislocations, the behavior of which after their occurrence hardly differs from the behavior of randomly formed dislocations. The author extended the ideas developed by him earlier to describe the formation of a cellular structure [55] to the description of the formation of a larger defect, which is the grain boundary.

V E Panin and his disciples proposed a theory of strongly excited atom-vacancy states in a solid [56]. The authors give a peculiar interpretation to the fact known from thermodynamics that a nonequilibrium (highly excited) system should be characterized by a large set of independent parameters [57]. The authors for the first time expressed and substantiated the conclusion that, under conditions of strong excitation, the state characterized by the maximum of the nonequilibrium thermodynamic potential should be taken as the initial one. This conclusion quite correctly agrees with the fundamentals of NET, in which stable stationary states are also associated with the maxima of some nonequilibrium thermodynamic potentials in the form of effective internal energy [58].

Among the studies that are close to the NET concept in their ideological foundations, Refs [59, 60] should be noted. The kinetics of the formation of structural levels in this approach is based on the principles of self-organization and the use of a three-parameter system of Lorentz equations, which were originally intended to describe other physical phenomena. The general theory was mainly used to describe a phenomenon close in nature to MPD (for modeling ultrafine lubrication).

Among other methods for modeling processes that occur during MPD, we can note the refinement void accumulation (RVA) method [61]. Here, from simple heuristic considerations, a system of kinetic equations is postulated for the main characteristics of the process, while the limiting value of the average grain size (deformation fragment) is actually introduced as a separate determining parameter, rather than derived as a solution to the system of kinetic equations. In addition, we can note the method of mesoscopic nonequilibrium thermodynamics [62].

It is possible to consider the fragmentation phenomenon within the framework of NET by analyzing the dependence of the internal energy on its structural parameters and to predict the fragmentation effect within the framework of the 'two-defect' model [29]. At a certain MPD stage, intense multiplication of dislocations occurs, which become a building material for the growth of the volume density of grain boundaries (deformation fragments). This leads to structure refinement under conditions where two types of defects (dislocations and deformation fragments) are mainly involved in MPD processes. Later, a 'three-defect' model was developed, where microporosity was taken into account as an additional structural defect [35].

The system of evolution equations (5) can be written in the explicit form [30, 63]

$$\frac{\partial h_D}{\partial t} = \gamma_D(\varphi_{0D} - \varphi_{1D}h_D + \varphi_{gD}h_g) + f_D\,, \tag{6}$$

$$\frac{\partial h_g}{\partial t} = \gamma_g(\varphi_{0g} - \varphi_{1g}h_g + \varphi_{2g}h_g^2 - \varphi_{3g}h_g^3 + \varphi_{gD}h_D) + f_g\,. \tag{7}$$

Here, the transition to the effective potential of internal energy $u_{\text{eff}} = u - \varphi_{ms}h_m$ has been carried out [63, 64]. In addition, regular or random sources of defects of the appropriate type are added to the right-hand sides of the equations for generality. With their help, one can simulate the effect of ultrasound or the impact of stochasticity on the activation of the processes of generating structural defects. Hereinafter, we assume $f_D = f_g = 0$.

Equating the right-hand sides to zero, we obtain the conditions for finding stationary values of the density of structural defects:

$$\begin{aligned} &\varphi_{0D} - \varphi_{1D}h_D + \varphi_{gD}h_g = 0\,,\\ &\varphi_{0g} - \varphi_{1g}h_g + \varphi_{2g}h_g^2 - \varphi_{3g}h_g^3 + \varphi_{gD}h_D = 0\,. \end{aligned} \tag{8}$$

Each term in Eqns (6), (7) models a certain level of the thermodynamic process during MPD. The positive terms are responsible for the generation of structural defects, and the negative terms are responsible for their annihilation. The alternation of signs implements the principle that a thermodynamic process of a higher level is directed against a process of a lower level. The signs of the coefficients can change during the evolution of the system, which corresponds to a

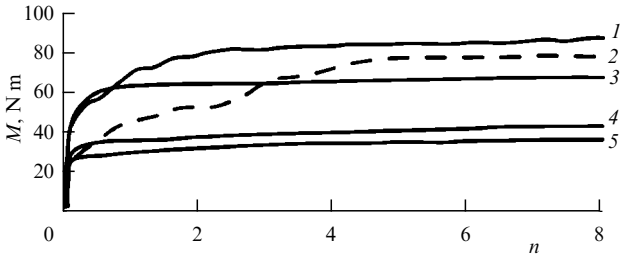

Figure 4. Change in torque M during HPT process at a pressure of 3 GPa; *1* — brass (Cu – 42% Zn); *2* — compact of a mixture of powders Cu + 42% Zn; *3* — copper; *4* — aluminum; *5* — zinc [66].

structural transition, e.g., from states with coarse grains to states with fine grains.

The presence of plastic flow predetermines the existence of a permanent source of structural defects (the first positive terms in Eqns (6) and (7)). With an increase in the density of structural defects, the degree of nonequilibrium in the system also increases, which leads to the initiation of oppositely directed relaxation processes (the second negative terms in Eqns (6) and (7)). These include, e.g., low-temperature recrystallization.

As the density of structural defects increases, the role of higher-degree contributions in Eqns (6) and (7) increases. First, the processes of low-temperature recrystallization are activated, which are proportional to φ_{1D} and φ_{1g}. Then, in the case of grain boundaries, the higher-level processes of fragmentation and recrystallization are activated, proportional to φ_{2g} and φ_{3g}, associated with the contribution of disclinations [65]. The transition from a coarsely fragmented structure, formed due to the contributions of φ_{0g} and φ_{1g}, to a microfragmented structure, formed mainly due to the contributions of φ_{2g} and φ_{3g}, occurs relatively abruptly according to the phase transition scenario.

5.2 Absence of strain hardening stage

Figure 4 shows the curves of plastic flow under HPT conditions in a Bridgman chamber equipped with sensors that measure the torque $M = f(n)$, where n is the number of complete revolutions of the movable anvil in the Bridgman chamber (a measure of plastic deformation under MPD conditions). The measurements were carried out at room temperature and under a quasi-hydrostatic pressure of 3 GPa [66]. For the polycrystalline Cu – 42% Zn alloy (brass), as well as for copper, aluminum, and zinc, the strain hardening stage is completely absent, which is typical of MPD. Worth attention is the distinct fixation of the strain hardening stage during MPD in a mixture of copper and zinc powders under mechanoactivation conditions (see Fig. 4). This undoubtedly indicates, among other things, a noticeable difference in the nature of MPD and mechanoactivation processes. The main differences are that, during mechanoactivation, the level of external stresses is significantly lower than during MPD, but the processes of chemical interaction on the surface of individual powder particles are much more active than on the internal interfaces during MPD. Unfortunately, many researchers neglect this circumstance and actually identify two processes that differ markedly in their physicochemical nature [24, 51, 58].

The absence of strain hardening during MPD is, of course, associated with a significant increase in the efficiency of relaxation processes compared to those during ordinary macroscopic deformation [67]. From the kinetic dependences of the density of dislocations and the boundaries of deformation fragments, calculated using the NET (Fig. 5a), it can be seen that their dynamics are closely related. At the beginning of the MPD process, dislocations intensively multiply, and therefore the yield strength increases (Fig. 5b), as do the acting stresses. This prepares the conditions for initiating an increase in the density of fragment boundaries and provokes the onset of the corresponding structural phase transition. By the time this happens, the dislocation density has already reached a stationary plateau; however, due to the influence of the increased number of fragment boundaries, it again demonstrates positive growth dynamics. Dislocations 'react' to a sharp increase in the density of fragment boundaries, but somewhat more weakly than their growth at the initial stage of MPD.

The staging of deformation is also manifested in the change in the nature of the hardening law at different stages of the process. At the first stage (Fig. 5b, region *1*), the hardening law can be approximated by the Hall–Petch relation. In region *B*, which corresponds to the 'fastest' phase of deformation, the hardening law can be approxi-

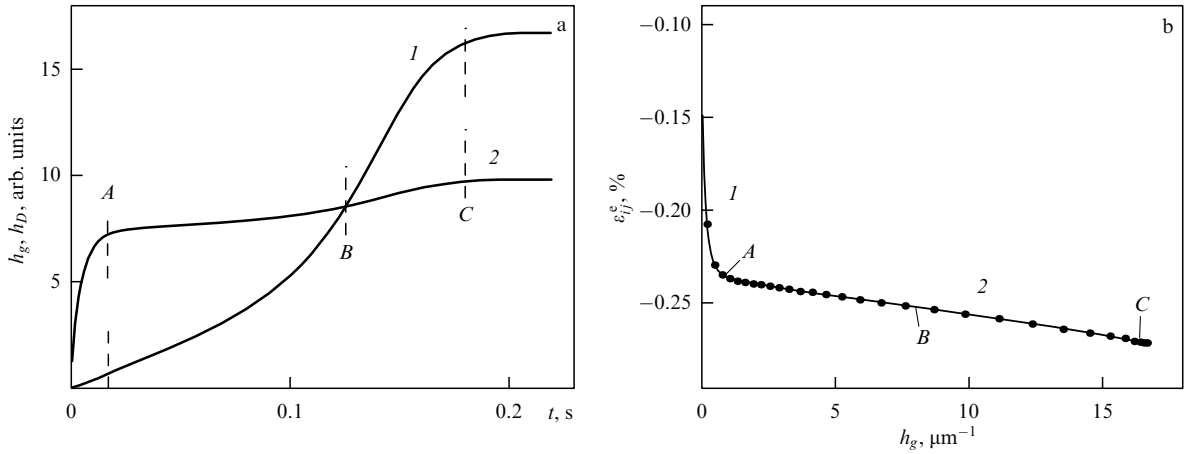

Figure 5. (a) Kinetics of changes in the density of defects (boundaries of deformation fragments (*1*) and dislocations (*2*)) during MPD. (b) Hall–Petch hardening law (*1*) and linear hardening (*2*). Points on the curves are plotted at regular time intervals; positions *A*, *B*, *C* indicate common fragments in plots (a) and (b) [67].

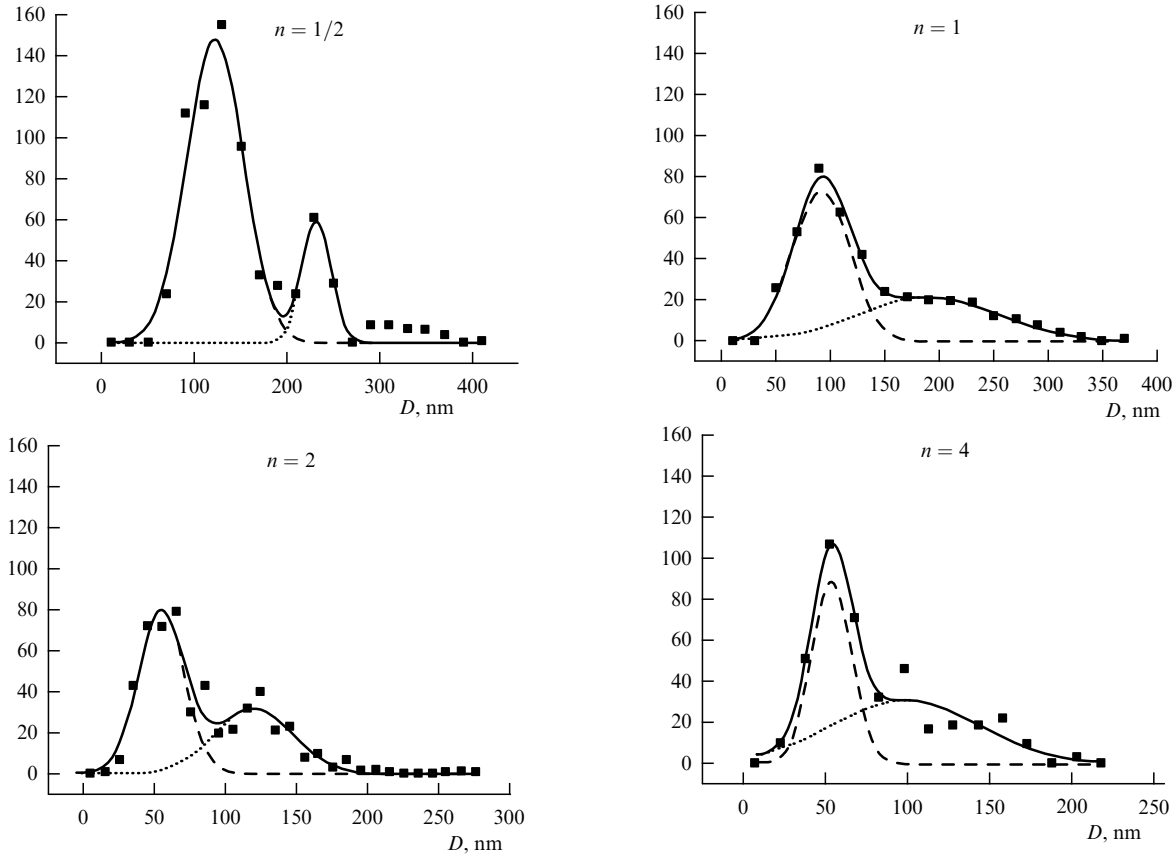

Figure 6. Non-normalized size probability distributions of recrystallized grains (RGs) and deformation fragments (DFs) and their separation into two Gaussian distributions after MPD with different numbers of total revolutions n for the FeNi alloy (50N). Solid line — total histogram, dashed line — DF, dotted line — RG [77].

mated by a linear dependence. It is this character of the change in the hardening law depending on the stage of deformation that was noted in experiment [65, 68]. The rate of the process within the framework of the revealed patterns of hardening is not the same. At the initial stage, when there is an intense multiplication of dislocations (to the left of point A), the process proceeds rapidly, then, after the dislocation density reaches a stationary regime (in the region of point A), it slows down. At the stage of intensive reproduction of fragment boundaries (in the region of point B), it accelerates again, and when the system reaches the stationary regime for both types of defects (point C), the process not only slows down but stops completely (point clustering, stationary state). Thus, although the slope of the curve as a whole demonstrates the tendency of the system toward material hardening, the rate of this hardening at point C is zero, and, in fact, in the limiting (stationary) state, the strain hardening of the material is not observed. Thanks to feedback, the system acquires the features of synergy, which results in a self-consistent transition of the system to a steady state. In the steady state, the macroscopic parameters of the system, the density of structural defects, cease to change; the yield strength does not change, either, and further implementation of MPD does not lead to strain hardening of the material.

5.3 Low-temperature dynamic recrystallization

The literature contains a large amount of experimental evidence that dynamic recrystallization occurs during MPD under conditions of low diffusion mobility of atoms at room and even lower temperatures (noticeably below $0.3T_{\text{melt}}$) [69, 70]. In this case, the dynamic recrystallization process goes, as a rule, without the formation of nuclei of new grains [71] (in accordance with the terminology proposed in monograph [72], continuous dynamic recrystallization). In Ref. [73], the geometric concept of continuous dynamic recrystallization was considered as applied to conditions close to those that are realized during MPD.

A characteristic feature of the structure of metallic materials after MPD is the existence of large local misorientations corresponding to high-angle grain boundaries [74]. According to the general opinion, it is these boundaries that largely determine the unique properties of materials after MPD [75]. High-angle boundaries, as established, separate two types of crystal regions, different in their origin, formed during MPD: deformation fragments (DFs) and recrystallized grains (RGs) [76]. DFs are formed as a result of fragmentation processes (see Section 5.1), while RGs are formed as a result of continuous dynamic recrystallization directly during MPD.

Figure 6 shows histograms of the RG and DF size distributions obtained after MPD in a single-phase polycrystalline FeNi alloy (fcc solid solution) using a specially developed transmission electron microscopy (TEM) technique for various numbers of full revolutions n of a Bridgman chamber movable anvil [77]. The value $D = \sqrt{S}$, where S is the grain or fragment image area, was chosen as the characteristic size of a structural element. An analysis of all the obtained distributions shows the presence of two maxima

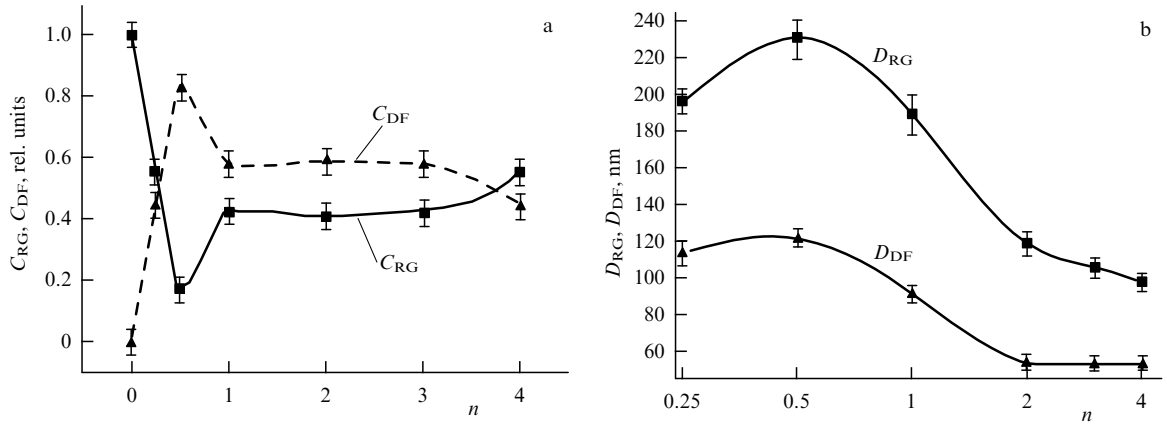

Figure 7. Changes in the volume fraction C_{RG} and C_{DF} (a) and the average size D_{RG} and D_{DF} (b) for recrystallized grains (RGs) and deformation fragments (DFs), respectively, depending on the number of complete revolutions n in the FeNi alloy (50H) [78].

(bimodal distribution), the parameters of which change depending on the deformation magnitude, while, however, the bimodal nature of the distributions is preserved.

Within the framework of one of the proposed basic concepts (see Section 3), during MPD, additional channels of relaxation (dissipation) of mechanical energy exist [22]. In addition, as we noted above, it was convincingly shown in a number of experiments that MPD processes at room temperature in metals and alloys are accompanied by dynamic recrystallization. Dark-field electron microscopic images of the structure clearly reveal individual grains that have the shape of almost regular hexagons and a low defect density. This testifies to the formation of such grains in the process of dynamic recrystallization by migration of high-angle boundaries or by cooperative rotation of individual fragments under conditions of a high concentration of point defects and large internal stress gradients [78]. At the same time, some areas (fragments) have an irregular shape and contain a high density of defects and noticeable local distortions, which certainly indicates their formation during deformation fragmentation [77].

The histograms presented in Fig. 6 are combined and consist of two histograms of the RG and DF distributions, which differ in their formation nature. It follows from the analysis of electron microscopic images [78] that the distribution indicated by dashed lines corresponds to DF, and the distribution indicated by dotted lines corresponds to RG. Then, by calculating the relative areas under the Gaussian distribution curves, the relative volume fraction occupied by deformation fragments C_{DF} and recrystallized grains C_{RG} was determined for each deformation mode (Fig. 7a), as was the average size of the regions corresponding to deformation fragments D_{DF} and recrystallized grains D_{RG} (Fig. 7b). With an increase in the number of movable anvil revolutions n, the value of C_{DF} first sharply increases, reaching 0.8, and then gradually decreases, corresponding to an almost constant (stationary) value of 0.6. The value of C_{RG}, which obviously includes not only recrystallized but also original grains, first sharply decreases to 0.2, and then increases to a value of 0.4, which also remains almost constant as n increases. The parameter $\kappa = C_{RG}/C_{DF}$ at $n > 1$ is an important structural constant and depends on the nature of the material and parameters of the MPD, determining to a large extent its physical and mechanical properties. In the process of MPD, a dynamic balance is observed between the structural transformations 'DF $\rightarrow$ RG.' Dependences $D(n)$, in accordance with Fig. 7b, have a symbate character: the values of D_{DF} and D_{RG} gradually decrease to 50 and 100 nm, respectively, and then, at $n > 2$, hardly change.

As the MPD magnitude increases, a strict linear correlation is observed between an increase in the proportion of grains formed during dynamic recrystallization and high-angle grain boundaries ($\varphi > 40^\circ$) measured by backscattered electron diffraction [79]. This result unambiguously indicates that it is the process of dynamic recrystallization, rather than deformational fragmentation, which is responsible for the formation of a sufficiently large number of high-angle grain boundaries in the structure of the material that has undergone MPD. Let us dwell on two important circumstances.

(1) The maximum in the distribution of high-angle grain boundaries occurs at disorientation angles $\varphi = 45^\circ - 55^\circ$, which correspond to the highest mobility of high-angle grain boundaries and, consequently, the most efficient growth of recrystallization nuclei [80].

(2) As the minimum value of φ decreases, when constructing the parametric dependences $\alpha(C_{RG})$ ($\alpha_{50} \rightarrow \alpha_{20}$), the linear correlation coefficient decreases [81], which certainly indicates an increasing contribution of dynamic fragmentation processes to the formation of grain boundaries with medium and small disorientation angles.

A sharp increase in the volume fraction of DFs, which are characterized by high magnitudes of internal stress fields, corresponds to an equally intense increase in the values of the coercive force H_c. Structure-sensitive strength and magnetic properties of single-phase materials that have been subjected to MPD are determined by the ratio of volume fractions attributable to DFs and RGs, $k = C_{DF}/C_{RG}$. The higher the value of k, the greater the strength (microhardness) and magnetic rigidity of the ferromagnet. In this work and in the study performed on commercially pure iron [76], the value of k turned out to be close to unity. It can also be assumed that an increase in the volume fraction of recrystallized grains (lower values of k) may correspond to an increase in the plasticity of materials subjected to MPD.

Thus, we can consider the structure after MPD as a 'two-phase mixture' consisting of DFs and RGs. Moreover, the presence of a high density of high-angle grain boundaries in the structure of the material that has undergone MPD is mainly due to dynamic recrystallization processes. Annealing of the 'two-phase mixture' structure leads to the occurrence of primary recrystallization processes, which lead to a signifi-

cant increase in the average size of the RGs, whereas the average size of DFs remains almost unchanged [82]. In fact, the primary recrystallization during annealing is realized due to an increase in the size of the RGs produced during MPD, while the DFs do not participate in this process. The reason is most likely that the DF boundaries form according to the disclination mechanism, are characterized by low mobility, and are not capable of active migration. DFs can take part in the process of primary recrystallization if they are preliminarily recrystallized, but by the coalescence mechanism rather than the boundary migration mechanism [72, 80]. Similar dependences within the framework of the 'two-phase mixture' model were obtained for FeCo – V [83] and Fe – Si [84] alloys and commercially pure titanium [85].

A question of extreme importance is what structural model describes the transformation of DFs, which have high internal stresses, into RGs, whose boundaries do not contain such stresses, directly during MPD under conditions of limited diffusion mobility. It was shown [86, 87] by computer simulation that the structure of DFs can be transformed under ultrasonic impact via a conservative rearrangement of dislocations and partial disclinations. Such a rearrangement, in fact, leads to the formation of RGs through the mechanism of continuous dynamic recrystallization. In the case of MPD, this process should be facilitated by the observed effect of a sharp increase in the diffusive mobility of atoms, the nature of which will be considered in Section 5.4.

5.4 Abnormally high diffusive mobility of atoms

As shown by numerous experiments, atomic diffusion during MPD is 10–20 orders of magnitude faster and occurs at a significantly lower temperature (to 77 K) than normal diffusion mass transfer under conventional thermal and deformation impacts [88, 89]. All attempts to analyze this unique phenomenon are based on classical models of diffusion acceleration in the presence of various kinds of stationary and migrating lattice defects [90]. As was theoretically shown in Refs [91, 92], with an increase in the MPD, a very large number of nonequilibrium point defects (vacancies and crowdions) are formed in the structure, which, under deformation, can stimulate diffusion phase transformations with accelerated diffusion of atoms along moving and stationary nonequilibrium grain boundaries, triple junctions, and individual dislocations [93–95]. Some phenomena of anomalous stratification and decomposition in individual alloys during MPD can be explained quantitatively in terms of diffusion through migrating defects, but this approach clearly ignores the fact that similar processes of defect migration, as a rule, also occur under ordinary macroscopic deformations, where, however, no anomalously high diffusion mass transfer was practically recorded. Among other things, under MPD conditions far from equilibrium, the diffusion laws are unlikely to be identical to those that operate under conditions close to thermodynamic equilibrium and were not quite correctly used in theoretical estimates [96].

The anomaly of diffusion mass transfer during MPD is obviously determined by the specifics of physical processes characteristic of strongly nonequilibrium states. Unfortunately, no fundamentally new models that are not related to the acceleration of diffusion on defects in a solid body have been proposed yet for MPD. Some exception is the phenomenological model formulated in Ref. [97] for irradiation processes and actively used in Refs [98, 99] to describe diffusion processes during MPD. Within the framework of the so-called 'ballistic' model, additional atomic jumps are postulated that stimulate diffusion and depend only on the intensity of the external action under conditions of constant temperature. A consequence of this model is the existence of an effective temperature T_{eff}, describing the shift of the phase composition of a solid during MPD to the high-temperature region of the state diagram corresponding to the value of T_{eff} for a given chemical composition. For example, the shift of T_{eff} to the region of the state diagram above the solidus line means that during MPD an amorphous phase should form [98].

In accordance with the basic principles of NET (see Sections 3 and 4), the deformation system in our case is open and obeys the laws of nonequilibrium thermodynamics [100]. As a result, additional channels of mechanical energy relaxation arise, among which the processes of thermal energy release play an important role. This leads to a local and short-term increase in temperature, which, in turn, can cause an abnormally high diffusion mass transfer. Theoretical and experimental estimates show that local and short-term (a few microseconds) temperature rises can reach several hundred degrees and thus significantly accelerate diffusion processes [101, 102]. Another possible reason for the anomalously high diffusion mobility of atoms during MPD is associated with very high gradients of elastic stresses and strains that arise during giant plastic deformations [103]. Apparently, additional estimates are required, based on experimentally established gradients, which could lead to an acceleration of diffusion during MPD, similar to the effects of 'upward' diffusion. It is possible that the colossal deformations that occur during MPD can give rise to fundamentally new mechanisms of atomic diffusion, which are directly related to the collective modes of plastic deformation.

The question of a dissipative increase in temperature during MPD is debatable. Some researchers believe that the effect of temperature increase certainly exists and should be taken into account [104, 105], while others believe that it is absent or negligible [98, 106]. The undoubted rightness of the first group of researchers has been proven by numerous experiments, among which it is worth distinguishing the work performed on amorphous alloys, where an increase in temperature in highly localized (and therefore highly distorted) deformation shear bands leads to 'reference points' — crystallization effects [107].

5.5 Cyclic character of structural phase transformations

The classical understanding of plastic deformation is based on the fact that the higher the degree of plastic deformation, the more defects the deformed crystal must contain [108]. The first exception to this rule arose during MPD with the active participation of disclination modes: the fragments had thin boundaries and were almost completely free of dislocations [109]. However, upon proceeding to the MPD region, cardinal structural transformations occur due to the activation of additional channels for mechanical energy dissipation. The authors of Ref. [110] reported a jump-like change in the structure and properties upon the transition to MPD. If we consider a particular microvolume of a deformed sample, then, after dynamic recrystallization or amorphization, the process of plastic deformation begins, as it were, 'from scratch' in the newly formed recrystallized grain or in the region of the amorphous phase. Furthermore, in the microvolume under consideration, under the action of deforming

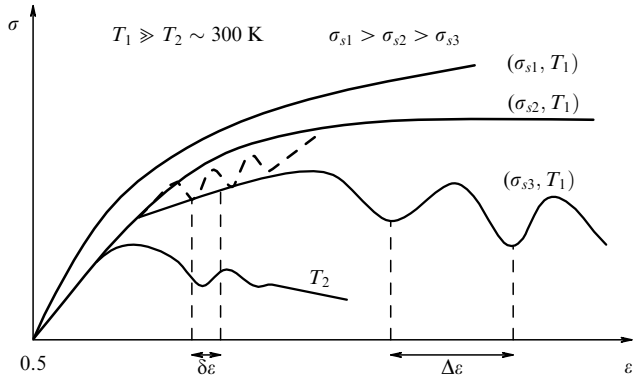

Figure 8. Possible types of strain curves at the MPD stage for materials with different Peierls barriers σ_s at different temperatures [111].

stresses, the accumulation of defects again occurs and the process is repeated.

Figure 8 shows the calculated curves of plastic flow, which take into account the existence of a dissipation channel and were obtained for materials with different degrees of dislocation mobility at different temperatures [111]. It is seen that, at low values of the Peierls barrier σ_s and in the presence of an effective dissipation channel, the plastic flow curve has a cyclic character with a 'wavelength' $\Delta\varepsilon$. The fact that we practically never record such flow curves in experiments does not contradict this consideration. The process of plastic flow at all stages of its development is extremely inhomogeneous, and simultaneously different regions of a deformable crystal are at different stages of their evolution.

Here, we should pay special attention to the results of a rarely cited paper by V A Likhachev et al. [112], which reported the MPD of copper wire ($e = 1.6$ and 3.7). The authors of [112] observed a cyclicity in the structure change as the deformation increased: fragmented structure ($d = 0.2$ μm) → recrystallized structure → fragmented structure ($d = 0.1$ μm), where d is the average size of fragments. It is interesting to note that the fragmented structure of the 'second generation' was twice as dispersed as compared to the structure of the 'first generation.' In principle, this implies the achievement of a nanostructural state ($d \leqslant 0.1$ μm) in the third and subsequent cycles.

Let us consider the 'road map' implemented in the MPD of pure metals and solid solutions [68, 113]. The passage of a deformable system to the stationary regime can follow two possible scenarios. In the first case, the processes of deformation fragmentation and dynamic recrystallization are completely balanced, and the system monotonically tends to its stationary state. In the second case, complete equilibrium is not achieved, and the fragmentation processes first outpace the processes of dynamic recrystallization, and then, on the contrary, somewhat lag behind them, which leads to an oscillatory evolution of the deformed system.

If the relaxation of excess mechanical energy occurs locally, regardless of relaxation (dissipation) in other domains of the solid, then in general it will have a continuous, monotonic character, and the system will evolve directly into its equilibrium state according to the first of the above scenarios. If the relaxation has a correlated avalanche-like character, so that the transition to the equilibrium state in one region of the solid body synchronizes the transition of parameters and variables to the equilibrium values in other stressed regions, then the solid will effectively relax, after

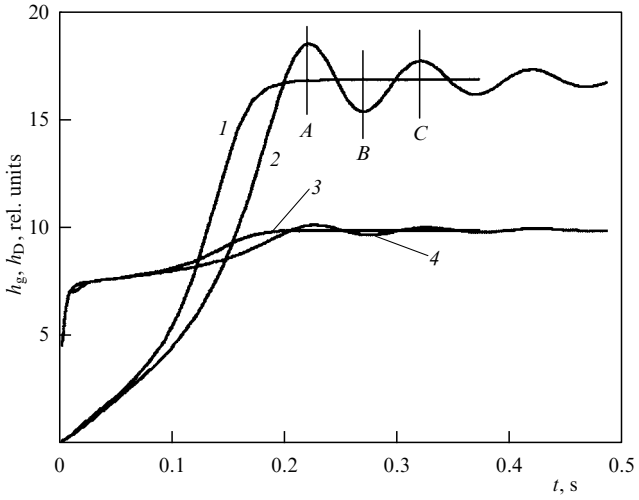

Figure 9. Kinetic curves for the formation of various types of defects; *1*, *2* — density of grain boundaries, *3*, *4* — density of deformation fragments, *1*, *3* — without prehistory, *2*, *4* — with prehistory; *A*, *B*, *C* — extreme values [68, 113].

which the new stage of mechanical energy accumulation for the next jump-like transition will begin. If this process is sufficiently pronounced, the relaxation will have an oscillatory periodic character, in accordance with the second of the above scenarios (see Fig. 8).

To describe such oscillatory transitions based on NET, a model of evolution equations with inertia (memory) was proposed [68, 113] (Fig. 9). In the first approximation, such a model can be applied to describe the phenomena associated with the periodicity of the processes of deformation fragmentation and recrystallization of grains. With the effects of memory (inertia) during strain structure formation taken into account, the main relations take a form characteristic of wave equations with damping. In the approximation of a unimodal grain size distribution, the deformation system gradually, performing damped oscillations, reaches a stationary value of the structural parameters. In this case, not only the structural parameters but also the strength properties of the material change cyclically during MPD.

The authors of Ref. [114] managed to detect the cyclic nature of the structural phase transformation crystal–amorphous state in the $Ti_{50}Ni_{25}Cu_{25}$ alloy upon MPD. Earlier, a similar effect was found in experiments on mechanical activation of Co_3Ti intermetallic powder [115]. Such cyclicity, i.e., the tendency to a phase transition from a crystalline state to an amorphous state and vice versa, explains, in our opinion, the apparent contradiction in the experimental results of Refs [116–118], on the one hand, and Refs [119–121], on the other hand.

It is assumed in the literature that the periodicity of structural changes during MPD is generally determined by the activation of various channels of dissipation (relaxation) of the mechanical energy stored by the material in the course of deformation [111]. Obviously, the specific features of the change in the structure of the $Ti_{50}Ni_{25}Cu_{25}$ crystalline alloy upon MPD found in [122] are related to the features of both diffusion and martensitic direct and reverse phase transformations.

In the $Ti_{50}Ni_{25}Cu_{25}$ crystalline alloy, during increasing deformation in a Bridgman chamber, the following sequence

of phase transitions is observed:

$$B19 \rightarrow \text{AS} \rightarrow B2 \rightarrow B19 \rightarrow \text{AS} \rightarrow B2\,, \qquad (9)$$

where AS is the amorphous state of the solid.

Scheme (9) gives insight into the nature of cyclic transitions during MPD from a crystalline state to an amorphous state and then from amorphous to nanocrystalline, followed by periodic repetition of processes, but already at the nanoscale level. Further studies made it possible to conclude that it is necessary to take into account not only the value of the average strain but also its strong inhomogeneity along the sample radius [123].

Due to the structural inhomogeneity of strain, cyclic amorphous–crystalline phase transitions can be 'mismatched' in the volume of the deformed material, since they simultaneously occur in regions with different values of plastic deformation. To get information about the change in the local structures of a cylindrical sample at different distances from its center during HPT in a Bridgman chamber, a study was carried out [123] using spatially resolved X-ray diffraction at six points along the radius of the deformed sample. Synchrotron radiation [124, 125] with a wavelength $\lambda = 0.688862$ Å and a beam size of 350×350 μm^2 was used.

The data shown in Fig. 10 indicate that, during HPT, regions with different contents of the crystalline phase volume fraction can be simultaneously present in one sample. With an increase in strain, the entire sample, on average, transforms almost completely into the amorphous state after $n \geqslant 4$. However, with a further increase in strain to $n \geqslant 6$, the picture changes noticeably [122]. With an increase in true strain in the initially crystalline $Ti_{50}Ni_{25}Cu_{25}$ alloy to $e = 3.5-4.0$ ($n = 6-7$), splitting of the X-ray amorphous halo is observed (Fig. 11).

The diffraction pattern is a superposition of at least three diffuse crystal reflections, the broadening of which is associated both with the small size of the crystals and with their deformation distortions. Blurred reflections belong to the $B19$ phase, which indicates the active development of the $B2 \rightarrow B19$ martensitic transformation during MPD. With a further increase in deformation to $n = 8-9$ ($e = 5.3$), the process of martensite degradation and the transition to an amorphous state begins again.

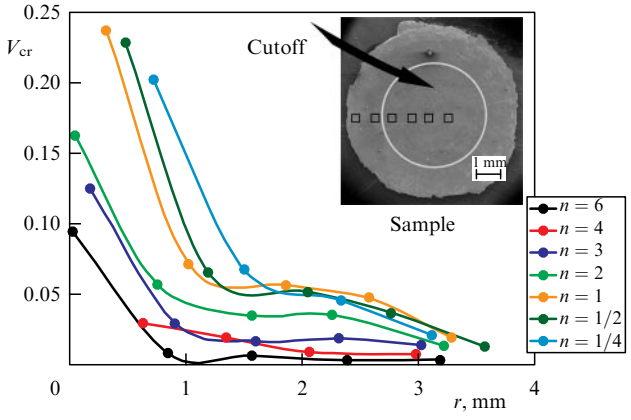

Figure 10. Change in the volume fraction of crystals V_{cr} depending on distance from the center to the edge of each sample after HPT of the $Ti_{50}Ni_{25}Cu_{25}$ alloy; inset shows an image of the sample with indication of the points of diffraction pattern acquisition with spatial resolution [123].

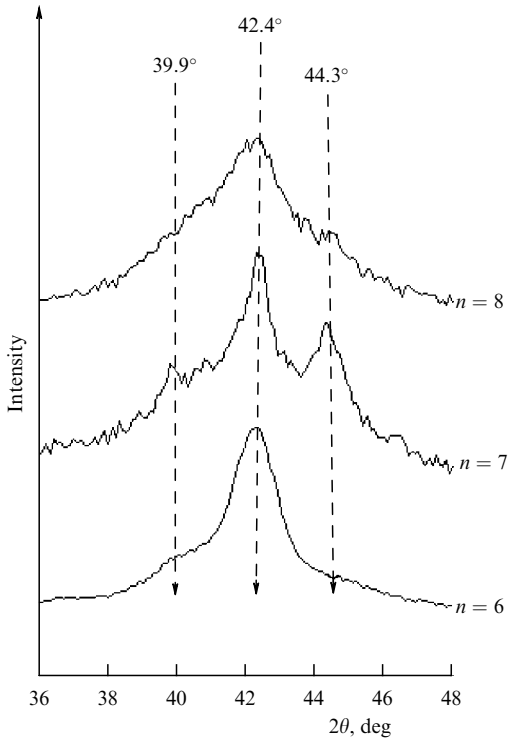

Figure 11. Splitting of the X-ray amorphous halo in the initially crystalline $Ti_{50}Ni_{25}Cu_{25}$ alloy after HPT ($n = 6-8$) obtained using radiation from a copper anode at room temperature [122].

Comparing the experimental results of Refs [126] and [122], we can state that the cyclicity detected during MPD has a damping character. As the deformation increases, the degradation of both the crystalline and amorphous states reaches a high degree. The so-called 'marginal' phase is formed in the alloy [127], i.e., an amorphous phase containing a certain number of nanocrystals.

Similar effects of deformation-induced cyclic phase transitions like the dissolution–nitride precipitation type in the surface layers of Fe–Cr–Ni–N alloys were found in Ref. [128].

5.6 Reversibility of structural phase transformations depending on temperature and severe plastic deformation parameters

In Ref. [129], using extended X-ray absorption fine structure (EXAFS) spectroscopy, the effect of temperature during HPT on the atomic structure and thermal effect of crystallization of amorphous $Fe_{83-x}Ni_xB_{17}$ alloys obtained by melt quenching was experimentally found. It has been established that HPT at 293 K leads to a decrease in the thermal effect of crystallization, and HPT at 77 K, on the contrary, leads to its increase, regardless of the alloy composition. Structural studies have shown that HPT at 298 K leads to a more ordered limit (stationary) state of the system (partial crystallization) of the initial amorphous alloys. On the contrary, HPT at 77 K forms a more 'ideal' amorphous structure (no short-range order and increased values of coordination numbers of iron atoms in the first coordination sphere). In other words, a change in the MPD deformation temperature leads to a kind of structural reversibility of the process, depending on whether the stationary state at a given

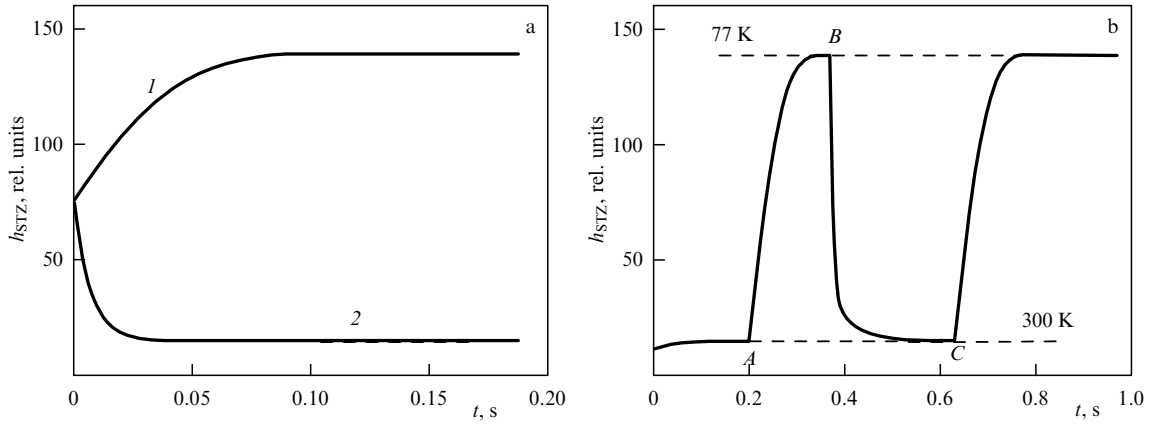

Figure 12. Evolution of the density of shear bands in an amorphous alloy during MPD at 77 K (*1*) and 300 K (*2*) (a) and upon a change in the deformation temperature at time moments *A*, *B*, and *C* (b) [82].

temperature has a higher or lower energy relative to the initial state of amorphous alloys after quenching from the melt. The structural reversibility of the processes of dissolution and precipitation of phases depending on the HPT temperature was also found in the precipitation of excess phases in crystalline solid solutions based on Fe–Ni [130] and Cu–Ag [131].

The internal energy of an amorphous material can be written as

$$u(h_{STZ}, h_v) = u_0 + \sum_{m=STZ,\,v} \left(\Phi_{0m} h_m - \frac{1}{2} \Phi_{1m} h_m^2 \right) + \Phi_{STZv} h_{STZ} h_v \,, \qquad (10)$$

where u_0 is the internal energy of a 'defect-free' amorphous material; h_{STZ} is the density of shear bands [132] or local zones of shear transformation [133, 134], which are, in fact, analogs of mesoscale dislocations; h_v is the vacancy density; and Φ_{0m}, Φ_{1m}, Φ_{STZv} are the coefficients in the power representation of the internal energy. The last may depend on stresses (elastic deformations) and on temperature.

Based on the principle of maximum nonequilibrium thermodynamic potential (10), we can proceed to a system of Landau–Khalatnikov evolution equations for the density of each type of defect:

$$\frac{\partial h_{STZ}}{\partial t} = \gamma_{h_{STZ}} (\Phi_{0STZ} - \Phi_{1STZ} h_{STZ} + \Phi_{STZv} h_v) \,, \qquad (11)$$

$$\frac{\partial h_v}{\partial t} = \gamma_{h_v} (\Phi_{0v} - \Phi_{1v} h_v + \Phi_{STZv} h_{STZ}) \,. \qquad (12)$$

As a result of evolution from an arbitrary nonequilibrium state, the system comes to a certain stationary state:

$$h_{STZ}^{(st)} = \frac{\Phi_{0v}\Phi_{STZv} + \Phi_{1v}\Phi_{0STZ}}{\Phi_{1v}\Phi_{1STZ} - \Phi_{0STZ}\Phi_{STZv}} \,, \qquad h_v^{(st)} = \frac{\Phi_{0STZ}\Phi_{STZv} + \Phi_{1STZ}\Phi_{0v}}{\Phi_{1STZ}\Phi_{1v} - \Phi_{0v}\Phi_{STZv}} \,. \qquad (13)$$

To model the regularities found experimentally in Ref. [129], one should take into account the temperature dependence of the coefficients in the potential expansion (10). We assume that the coefficients Φ_{1STZ} and Φ_{1v}, which are responsible for annihilation of defects, depend most strongly on temperature. Since the diffusion of atoms, which increases with temperature, plays an important role in the annihilation of defects, we assume that

$$\Phi_{1STZ} = \Phi_{1STZ}^0 (1 + \alpha T) \,, \qquad \Phi_{1v} = \Phi_{1v}^0 (1 + \alpha T) \,, \qquad (14)$$

where Φ_{1STZ}^0, Φ_{1v}^0, α are coefficients.

It follows from Eqns (13) and (14) that, at $\alpha > 0$, lower temperatures in the steady state correspond to higher densities of defects, such as shear bands. If, as a result of quenching from the melt, the initial density of defects turns out to be lower than its stationary value at a given temperature, then the density of defects will increase (Fig. 12a, curve *1*); otherwise, it will decrease (Fig. 12a, curve *2*).

An increase in the density of shear bands (curve *1*) leads to a higher degree of amorphization of the alloy and to an increase in the average values of the coordination numbers in the first coordination sphere around the iron atoms. On the contrary, a decrease in the density of shear bands (curve *2*) lowers the degree of amorphization and leads to a more ordered state up to partial crystallization of the initial amorphous alloys.

A change in temperature directly during deformation leads to an alternation of stationary states (Fig. 12b). First, processing at a temperature of 300 K (to the left of point *A*) is simulated. The system goes from an arbitrary state to an asymptotic (stationary) level. At point *A*, the material is already deformed at a temperature of 77 K, and the system reaches a higher asymptotic level corresponding to a higher density of shear bands characteristic of a lower temperature. At point *B*, the deformation is again carried out at room temperature, and the system returns to the previous asymptotic level. Finally, at point *C*, the processing is carried out again at a cryogenic temperature, and the system again reaches the asymptotic level characteristic of a low temperature. Similar regularities were also observed during MPD of polycrystalline fcc alloys [135]. It was possible to achieve a small grain size at significantly lower deformations. The subsequent MPD of the same material at room temperature no longer led to a decrease but, on the contrary, to an increase in the average grain size.

Calculations show that at each MPD temperature, its own limit structure (stationary state) is formed. At cryogenic temperatures, a structure with a higher density of mesoscale dislocations (shear bands) is produced, which leads to a

higher degree of amorphization than the initial state. At room temperature, the process develops in the thermodynamically opposite direction and leads in our case to ordering effects.

5.7 Amorphization of crystalline phases and crystallization of the amorphous state

5.7.1 Deformation nanocrystallization. In early papers [136] devoted to the study of structural changes in amorphous materials under severe plastic deformations, it was shown that, under these conditions, nanocrystallization of the amorphous phase occurs: nanocrystals 10–20 nm in size are observed homogeneously or heterogeneously distributed in the amorphous matrix. The appearance of nanocrystals uniformly distributed over the entire volume of the amorphous matrix at room temperature is difficult to explain in terms of classical concepts of the thermally activated nature of crystallization processes. In this regard, an attempt was made to analyze in detail the features of the structure and properties under the action of HPT on a number of amorphous metal–metalloid alloys, obtained by quenching from a melt ($Ni_{44}Fe_{29}Co_{15}Si_2B_{10}$, $Fe_{74}Si_{13}B_9Nb_3Cu_1$ (Finemet), $Fe_{57.5}Ni_{25}B_{17.5}$, $Fe_{49.5}Ni_{33}B_{17.5}$, $Fe_{70}Cr_{15}B_{15}$) and $Ti_{50}Ni_{25}Cu_{25}$ [36, 137, 138]. Thus, for example, in Ref. [137], under an HPT with $n \leqslant 2$ in the $Ni_{44}Fe_{29}Co_{15}Si_2B_{10}$ alloy, inhomogeneous plastic deformation is observed with the formation of coarse shear bands, which is inherent in the deformation of all amorphous alloys at temperatures significantly below the point of transition to the crystalline state. Local shear bands (SBs) were observed by transmission electron microscopy in samples after HPT at room temperature due to crystallization occurring in them (Fig. 13). Otherwise, the contrast in the electron microscopic image may only be of an absorption nature and not appear after the preliminary operations of preparing thin foils for electron microscopic analysis.

The question arises as to the possibility of the appearance of a crystalline phase at temperatures substantially below the transition point to the crystalline state. It was assumed that, in the course of a nonuniform deformation under HPT, there is short-term local heating in the SB regions.

As a rule, experimental attempts to estimate the temperature increase under HPT conditions are reduced to determining the average temperature of the entire sample. Reference [139] presents the results of temperature measurements in a stainless steel sample during HPT at room temperature. The thermocouple was located at a distance of 1 mm from the sample. At a twisting rate of 0.2 rpm, an increase in temperature ΔT of 10 K was recorded. At a twisting rate of 5 rpm, ΔT reached 200 K.

In more recent studies, including both direct temperature measurement near the sample surface and its simulation [104, 105], it was found that the temperature increase during HPT processing depends both on the nature of the material and on the deformation parameters. The stronger the material, the higher the applied hydrostatic pressure, the higher the rotation speed, and the greater the distance from the center of the sample, the greater the value of ΔT.

As to amorphous materials, we should first of all mention the classical and widely discussed experiment described in Ref. [140]. Before bending deformation, the authors deposited a fusible material on the surface of an amorphous alloy sample. Thus, the fact of strong heating of the material exactly in the SB zone was qualitatively established. In addition, a number of weighty pieces of evidence have been accumulated that a noticeable local increase in temperature is observed in the SBs of amorphous materials during deformation. For example, the authors of Ref. [141], using finite element modeling, came to the conclusion that, when massive steel samples are compressed at a speed of 10 m s^{-1}, the temperature of the entire sample can be somewhat higher than 150 °C, while the temperature in the SBs can exceed the average sample temperature by several hundred degrees.

Theoretical estimates [107] show that a local and short-term (no longer than a few microseconds) temperature increase in SBs can reach 500 °C. In this case, the local temperature in the plastic shear zone can exceed the crystallization temperature of some amorphous alloys and lead to the formation of a crystalline phase in the SB. It is important to emphasize that the manifestation of such effects is observed, as a rule, during deformation at room temperature under MPD conditions, when SBs realize a very high local power of plastic shear.

This assumption is confirmed by the results of [126], where amorphous iron-based alloys with close chemical compositions but different crystallization temperatures (T_{cr}) were deformed using HPT under the same conditions ($n = 1$, $P = 4$ GPa, room temperature). It was experimentally found that, the lower the value of the crystallization temperature of an amorphous alloy, the greater the value of the volume fraction (V_{cr}) of the crystalline phase observed after HPT under the same deformation conditions (Fig. 14). Based on

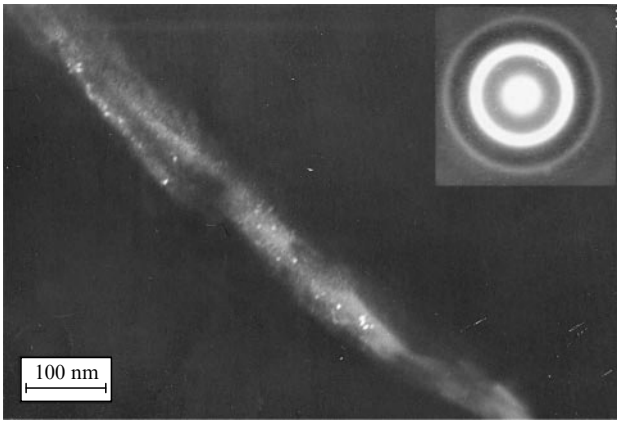

Figure 13. Electron microscopic image of a crystallized local shear band in the amorphous alloy $Ni_{44}Fe_{29}Co_{15}Si_2B_{10}$ after MPD ($n = 0.5$, $T = 293$ K) [137].

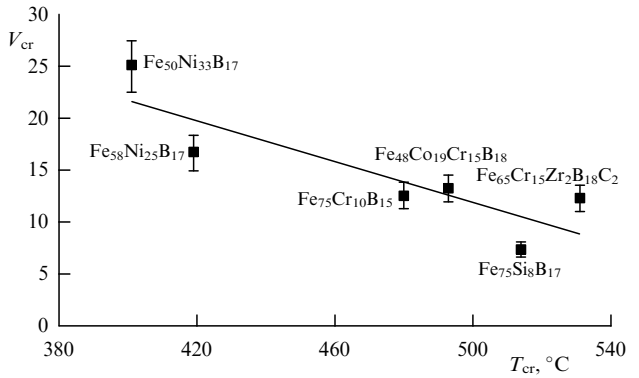

Figure 14. Correlation between V_{cr} and T_{cr} values for Fe-based amorphous alloys after HPT [138].

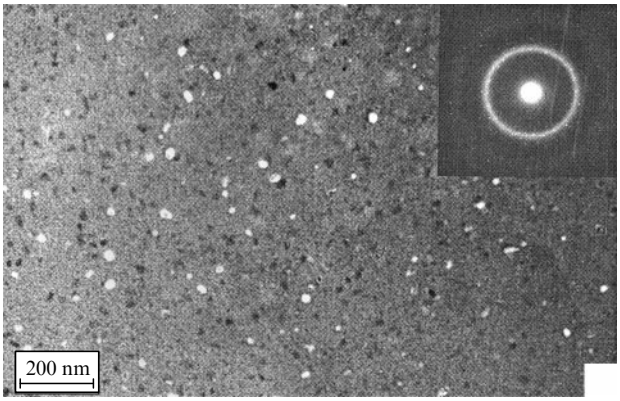

Figure 15. Dark-field electron microscopic image taken with the reflection from the nanocrystalline phase of an amorphous alloy $Ni_{44}Fe_{29}Co_{15}Si_2B_{10}$ after MPD ($n = 8$, $T = 77$ K) [145].

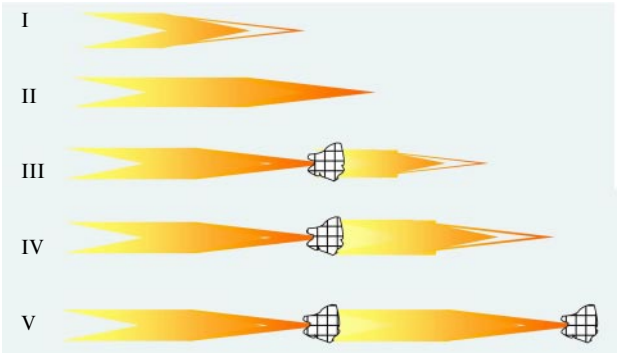

Figure 16. Mechanism of 'self-blocking' of a shear band propagating in an amorphous matrix [145].

the estimates made, it was suggested that the effect of crystallization in iron-based amorphous alloys upon HPT is due to both adiabatic heat release and a corresponding temperature increase in highly localized deformation SBs, as well as a noticeable increase in the concentration of regions of excess free volume.

A local and short-term increase in temperature was confirmed by the detected special character of the electron microscopic contrast in the amorphous structure and the change in the nanohardness values in the immediate vicinity of the SB location in amorphous alloys [142, 143]. In addition to a local increase in temperature, we cannot exclude the influence on the crystallization processes of an increased concentration of regions with excess free volume in shear bands, which was first recorded in SBs in Ref. [144].

During further development of the HPT in amorphous alloys with the accumulation of strain ($n \geqslant 2$), the picture changes dramatically [145]. Practically no SBs are detected. Instead, crystalline phase nanoparticles up to 10 nm in size are seen in the structure, homogeneously located throughout the sample volume (Fig. 15).

Apparently, the process of plastic deformation of amorphous alloys transforms from strongly localized and inhomogeneous to 'quasi-homogeneous.' As is known, a similar character of plastic flow is inherent in amorphous alloys at very high temperatures close to the glass transition point under conditions of a sharp decrease in the dynamic viscosity of the amorphous state [146]. A possible explanation for the observed delocalization of plastic flow is given in Ref. [145]: as an SB propagates in an amorphous matrix in the course of HPT, its temperature continuously increases, and, at the band propagation front, it is always maximum (I in Fig. 16). There comes a moment when the local temperature reaches the crystallization temperature (II in Fig. 16), and, as a result, a nanocrystal appears at the front of the growing band, which sharply slows down the plastic flow zone. Deceleration is associated with the nanosize of the resulting crystal, which, due to its smallness, is not capable of developing dislocation plastic flow. There are two options for further developments. First, under the action of the SB, the nanocrystal will accumulate a high level of elastic stresses, as a result of which a new SB will be generated in the amorphous matrix via the elastic accommodation mechanism (III in Fig. 16). In this case, plastic flow will proceed according to the relay-race mechanism, giving rise to the formation of nanocrystals in the SB, which are equidistantly located along the trajectory of the shear band in the amorphous matrix.

Further, the process of branching of SBs retarded due to the frontal formation of nanocrystals is possible. As a result of such 'self-deceleration' of the SB by frontally located nanocrystals, the inhomogeneous plastic flow is delocalized. In fact, the observed effect of the transition to homogeneous nanocrystallization on SBs means that plastic flow is characterized by a high bulk density of SBs, as a result of which a uniform precipitation of nanocrystals is observed in 'thinner' SBs. A similar plastic flow delocalization effect was found in a bulk amorphous alloy based on Zr [147].

From the point of view of the energy concept of MPD as a dynamic dissipative system [11] and the NET theory [17], the dissipation of significant mechanical energy introduced during HPT can include not only plastic deformation but also phase transformations and heat release as possible channels. It is known that the cause of crystallization is not only a local increase in temperature but also the presence of significant local stresses in the amorphous matrix. Stresses stimulate the occurrence of temperature-dependent processes, and, the higher the stresses, the lower the temperature for the implementation of thermally activated crystallization processes. In addition, it is necessary to take into account the fact that the value of the activation energy of the crystallization process is lower than usual due to the higher concentration of regions of excess free volume in the SBs [144]. It is quite possible that, even before the onset of crystallization, the amorphous matrix contains strain-induced regions with an increased correlation in the arrangement of atoms (nuclei of the crystalline phase with a markedly different degree of compositional and topological short-range order). This is indirectly evidenced by the results of Ref. [148], which show that the chemical composition of the crystalline phase in an amorphous aluminum-based alloy after conventional annealing and after HPT differ significantly. In Ref. [149], Mössbauer spectroscopy revealed the formation of short-range order regions (clusters) in bcc Fe–Mn alloys subjected to MPD.

To elucidate the character of the evolution of the local atomic structure in an amorphous matrix subjected to MPD and its effect on the thermal and magnetic characteristics of amorphous alloys based on Fe and Ti, a series of experiments was carried out using EXAFS spectroscopy with synchrotron radiation [150]. The analysis of the EXAFS spectra showed that HPT changes both the chemical environment of the selected Fe atom and the average interatomic distance of the Fe–Fe, Fe–Si, and Fe–Ni pairs. In $Fe_{58}Ni_{25}B_{17}$ and

$Fe_{75}Si_8B_{17}$ alloys, a change in the nature of the compositional short-range order for Fe atoms with a simultaneous decrease in the average interatomic distance for pairs of Fe–Fe atoms was found. In $Fe_{50}Ni_{33}B_{17}$ and $Fe_{54}Ni_{29}B_{17}$ alloys, no changes in the interatomic distances between different pairs of atoms were recorded. In these alloys, only a change in the chemical composition of the environment of the Fe atom was found: some of the Fe atoms were replaced by Ni atoms. Such changes in the local atomic structure usually lead to a decrease in the saturation magnetization in the studied amorphous alloys after HPT at 77 K. A sharp increase in the coercive force after HPT at 77 K is explained by the absence of elastic stress relaxation channels due to the suppression of thermal activation processes. It was shown in [129] that HPT at 77 K leads to the formation of an amorphous state more resistant to crystallization than after quenching from the melt.

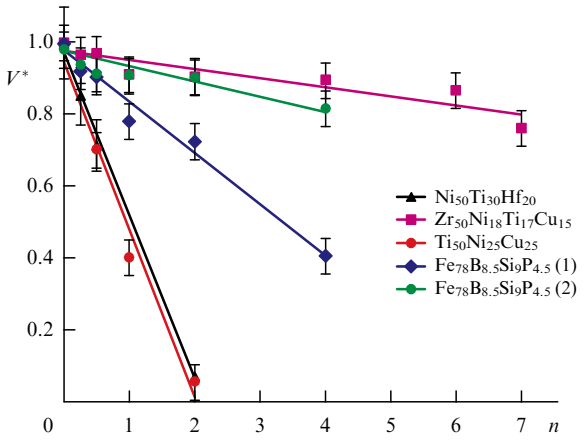

Figure 17. Reduced volume fraction of the crystalline phase V^* for the studied alloys versus the value of n [160].

5.7.2 Deformation-induced amorphization. The most common method for obtaining amorphous materials is quenching from the liquid state, during which glasses of various chemical compositions with various types of bonds are formed. However, not all melts transform equally easily into the amorphous state. Easily vitrifying liquids include covalent melts and polymer liquids, for which the critical process rate does not exceed 10–100 K s^{-1} [151]. Metal melts are much more difficult to amorphize; the critical glass transition rate for them is in the range of 10^5-10^{13} K s^{-1} [152].

The structure of amorphous materials is still the subject of discussion and research. A structure lacking long-range order can be obtained bypassing the liquid phase. For example, a very high concentration of defects (disclinations) [146] can be introduced into a crystalline material or it can be subjected to external impacts, e.g., by placing it in a high hydrostatic pressure chamber [9]. The results of an experimental study of the solid-phase amorphization under high pressure in a wide range of compounds ($Gd_2(MoO_4)_3$, $Tb_2(MoO_4)_3$, $Sm_2(MoO_4)_3$, $TbGd(MoO_4)_3$) were published in 1995 by a group of Russian researchers from the Institute of Solid State Physics, Russian Academy of Sciences [153]. A series of studies of the crystal structure of Si- and Ge-based semiconductors under high pressure, carried out at the Vereshchagin Institute for High Pressure Physics, Russian Academy of Sciences, made it possible to establish the patterns of solid-phase amorphization of high-pressure phases and to obtain bulk samples of these phases in the amorphous state [154].

When performing MPD using HPT, the high quasi-hydrostatic pressures affect metal crystals more effectively. Numerous defects of deformation origin arise, which leads as a result to the formation of new metastable phases and, in some cases, causes a phase transition to a metastable amorphous state.

In Ref. [123], EXAFS spectroscopy was used to compare the local atomic structures of an amorphous $Ti_{50}Ni_{25}Cu_{25}$ alloy obtained by melt quenching (MQ) and HPT at different MPD magnitudes in a Bridgman chamber. Studies have shown that the amorphous phase that appears under different strains is not identical to the one obtained by the MQ method. Moreover, the HPT-induced local atomic structure of the amorphous phase changes depending on the strain magnitude. It densifies and becomes more perfect as the strain magnitude increases at room temperature.

Structural and thermodynamic aspects of the process of deformation-induced amorphization during HPT are still the subject of lively discussion [17, 123, 155–157]. The most illustrative example is titanium nickelide TiNi, for which the transition to the amorphous state during HPT was recorded back in 1990 [158] and confirmed by further studies [118, 159].

It can be assumed that under HPT conditions a crystal containing a very high concentration of linear and point defects turns out to be thermodynamically unstable with respect to the transition to the amorphous state, especially if the difference between the free energies of the crystalline and amorphous states is small. As a rule, this process develops in multicomponent metal systems prone to amorphization (mainly based on Pd–Cu, Ti–Zr, Zr–Cu, Mg–Cu, TiNi–TiCu) [5].

A group of researchers from Kurdyumov Institute for Metal Physics (IMP) carried out a series of systematic studies of the main regularities of deformation-induced amorphization during HPT in multicomponent crystalline alloys. In Ref. [160], the amorphization process was studied in $Ni_{50}Ti_{30}Hf_{20}$, $Ti_{50}Ni_{25}Cu_{25}$, and $Zr_{50}Ni_{18}Ti_{17}Cu_{15}$ crystalline alloys in the initially single-phase state and in the $Fe_{78}B_{8.5}Si_9P_{4.5}$ alloy both in the initially single-phase (1) and initially two-phase (2) states. It should be noted that the selected alloys had different propensities for amorphization upon quenching from the liquid state. For all the investigated alloys, the change in the volume fraction of the crystalline phase V was determined by X-ray diffraction analysis.

The resulting dependence $V^*(n)$ is shown in Fig. 17, where $V^*(n)$ is the value of the reduced V, and n is the degree of deformation proportional to the number of revolutions of the movable anvil. The slope of the curves $k_c = |dV^*/dn|$ was taken as the parameter of the material's tendency to deformation-induced amorphization.

From Fig. 17, it follows that all the studied alloys can be conditionally divided into two groups:

(1) Alloys with a high value of k_c (the first group)—$Ni_{50}Ti_{30}Hf_{20}$, $Ti_{50}Ni_{25}Cu_{25}$, and $Fe_{78}B_{8.5}Si_9P_{4.5}$(1) in a single-phase state.

(2) Alloys with a low value of k_c (the second group)—$Zr_{50}Ni_{18}Ti_{17}Cu_{15}$ and $Fe_{78}B_{8.5}Si_9P_{4.5}$(2) in a two-phase state.

In the paper, the tendency to amorphization of individual phases that make up the alloys was also investigated. It was shown that the transition to the amorphous state of crystalline alloys during HPT is determined by the additive tendency to deformation amorphization of the crystalline phases included in their composition. Summing up the results

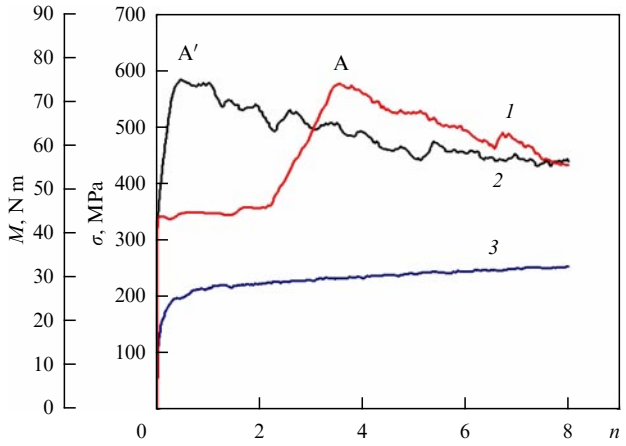

Figure 18. Continuous variation curves of torsional stresses $\sigma(n)$ calculated from data on the torque (M) recorded *in situ* during deformation of the $Ti_{50}Ni_{25}Cu_{25}$ alloy at room temperature: initially crystalline state (curve *1*), initially amorphous state (curve *2*), polycrystalline copper (curve *3*) [126].

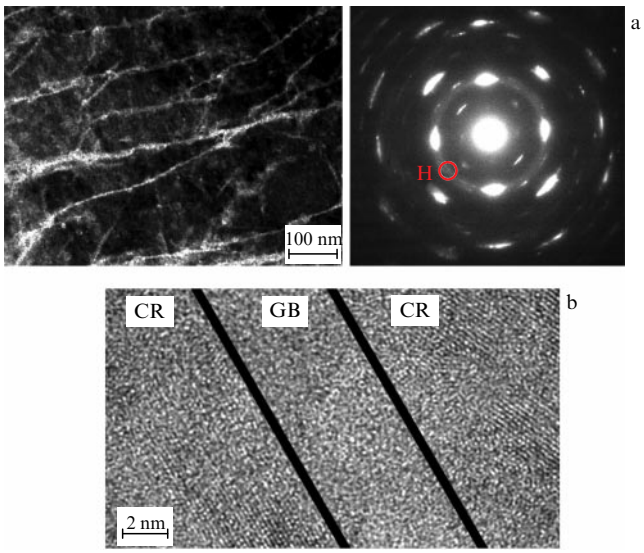

Figure 19. Electron microscopic images of the $Ti_{50}Ni_{25}Cu_{25}$ alloy structure after HPT ($n = 1/4$) demonstrating amorphous phase precipitation on crystal phase defects (dislocations and grain boundaries): (a) microscopic electron diffraction pattern and dark-field image using the first diffuse ring region (H); (b) image in the high-resolution TEM mode (CR — crystalline phase, GB — amorphous grain boundary) [167].

obtained, the authors concluded that the transition from the crystalline state to the amorphous one is generally determined by three factors:

(a) the tendency to accumulate deformation defects in the crystal under mechanical action;

(b) the degree of thermodynamic stability of the crystalline phases that make up the alloy;

(c) the tendency to diffusion processes, which are necessary to change the chemical composition of crystalline and amorphous phases during deformation.

It was also shown that the tendency to deformation-induced amorphization during HPT differs significantly from the tendency of the same alloys to amorphization by quenching from the liquid state. Obviously, this is due to the fact that the processes of amorphization during MPD and during quenching from the melt are controlled by absolutely different physical parameters. During quenching from the melt, they are the characteristics of the melt and the values of its glass transition temperature [161]. Such differences were experimentally confirmed in Ref. [162].

Of principal importance is the question of where and how the nuclei of the amorphous phase arise in the course of amorphization by HPT. In Ref. [126], the evolution of the $Ti_{50}Ni_{25}Cu_{25}$ crystalline alloy structure was analyzed by comparing the force parameters of deformation obtained during HPT *in situ* with the results of structural studies carried out after unloading the sample at different stages of deformation. Figure 18 shows curves of continuous change of torsional stresses $\sigma(n)$, calculated based on the torque (M) data, recorded *in situ* in the course of deforming the $Ti_{50}Ni_{25}Cu_{25}$ alloy at room temperature.

For the purity of the experiment, the studies were carried out by comparing the behavior of the same alloy in two states: amorphous, obtained by quenching from the melt (curve *2*, Fig. 18), and crystalline, obtained by annealing the initial amorphous state (curve *1*, Fig. 18). For comparison, the same figure shows curve *3* corresponding to the change in torsional stress $\sigma(n)$ for polycrystalline copper that does not undergo phase transformations during HPT.

Curve *1* was divided into 3 stages: *stage I* ($0 < n < 2$), at which the level of shear stresses in the material changes insignificantly, and the proportion of the amorphous phase increases to ~ 0.9; *stage II* ($2 < n < 4$), at which the level of shear stresses sharply increases from 350 to 574 MPa. Moreover, the values of maximum shear stresses σ_{max} for deformation curve *1* at $n \geqslant 4$ and for curve *2* (points A and A′, respectively) completely coincide. Further, at *stage III* of HPT ($n \geqslant 4$), $\sigma(n)$ gradually decreases from 574 MPa to 450 MPa. Hence, it follows that, at $n \geqslant 4$, the deformation behavior of the initially amorphous and deformation-amorphized alloys is comparable. In the course of further HPT deformation, the compared alloys behave similarly. The results of electron microscopic analysis of the $Ti_{50}Ni_{25}Cu_{25}$ alloy structure after HPT at 293 K showed that the average grain size of the crystalline phase decreases from 500–2000 nm in the initial state to $\sim 4-5$ nm at stage II of deformation ($n \geqslant 2$) [126].

It is known that under extreme deformation, in particular, during shear under pressure, the minimum size of nanocrystals can reach 10 nm [163]. On the other hand, at average grain sizes $\leqslant 10-20$ nm, the probability of the existence of developed dislocation modes in them is very low [164]. The theoretical possibility of a cardinal change in the deformation mechanism from intragranular to grain-boundary at a grain size $\leqslant 20$ nm was shown in Refs [165, 166]. Consequently, at a grain size $\leqslant 20$ nm, grain boundaries become the key element of the structure that determines the occurrence of plastic deformation. Experiments [167] have shown that low-temperature grain-boundary slip, associated grain displacements, and their mutual rotations are activated in the structure. From the condition of maintaining the continuity of the material, it follows that this process must be accompanied by the emission of deformation vacancies from triple junctions and steps at the grain boundaries into the body of the grain. Grain boundaries, which are not only sources but also sinks of defects, absorb vacancies, storing a non-equilibrium excess-free volume, and are partially amorphized (Fig. 19). Further deformation leads to multiple repetition of the process. The process is shown schematically

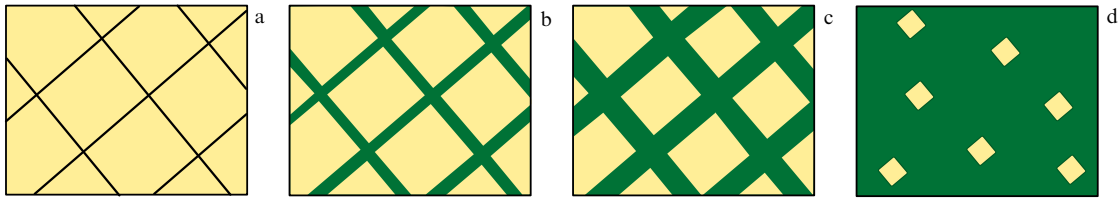

Figure 20. Schematic image of structural transformations during crystal → amorphous state transition during HPT: (a) structure fragmentation, (b) formation of amorphous boundaries (layers), (c) increase in proportion of amorphous layers, (d) amorphous-nanocrystalline state [126].

in Fig. 20. Vacancies flow through the grain volume and are absorbed in compressed areas of the boundary, as a result of which the boundaries expand [126]. The thickness of the 'grain-boundary' frame increases during HPT. It transforms into a massive amorphous phase, which occupies an increasing volume. The possibility of transformation of boundaries into the amorphous state during HPT was also shown in a number of papers on molecular dynamics modeling [168–170].

6. Deformation and accompanying phenomena during severe plastic deformation

As noted in Section 3, one of the basic principles of MPD is the division of all processes occurring during it into those that directly determine the deformation behavior of a solid and, in fact, represent its response to giant external impacts, and those that can be considered secondary and accompany them. Deformation processes are, as a rule, of an athermal nature. The accompanying processes, on the contrary, are controlled by diffusion and, therefore, have a thermal activation nature. The only exceptions are martensitic-type phase transformations. However, the activation energy plays a certain role for them, too. For example, in commercially pure titanium, a martensitic ω-phase appears at certain HPT stages [171]. However, in the case of HPT at room temperature, the critical deformation corresponding to the onset of the martensitic transformation $\alpha \rightarrow \omega$ is somewhat smaller than for HPT at cryogenic temperatures [172]. This certainly indicates that the transformation has a thermally activated component. In principle, the deformation and accompanying processes can proceed independently, but they can influence each other to one degree or another. For example, accompanying phenomena associated with a change in the phase or chemical composition during MPD can affect the propagation of plastic shear zones and other deformation modes of plastic deformation. In this sense, MPD experiments at different temperatures seem to be extremely productive, since thermally activated and athermal processes in this case will have a different effect on the thermodynamics and kinetics of deformation and accompanying phenomena, as well as on the nature of their mutual influence.

6.1 Deformation processes

6.1.1 Shear bands. The basic parameters of the collective modes of plastic deformation, which primarily include shear bands, determine the qualitative and quantitative characteristics of the plastic flow of a material at the stage of MPD [7, 108]. It seems to be a strong assumption to consider the mechanisms of deformation phenomena during MPD to be based on the behavior of individual defects (dislocations, stacking faults, vacancies, etc.). At such gigantic degrees of deformation, we can only speak of collective ensembles of interacting defects.

SBs can be studied most reliably and efficiently under MPD of amorphous alloys. Such SBs are, as a rule, highly localized and are, in fact, the dominant mode of plastic flow in disordered materials [132]. Recently, many papers have appeared that analyze the formation of shear bands during HPT of ribbon and bulk amorphous alloys obtained by melt quenching [173, 174].

It has been reliably established that SBs under both ordinary and megaplastic deformations are characterized by a very high degree of plastic shear localization (SB thickness is about 30–70 nm [144]). The amorphous state inside the SB has lower values of density [144, 175], the degree of short-range ordering [146], and the Young's modulus [178]. Detailed studies [143, 177–180], including *in situ* observations in a column of a high-voltage electron microscope [181], showed that, similarly to the dislocation flow in crystals at cryogenic temperatures [182], SBs in amorphous alloys form a system of coarse steps on a sample surface with a shear origin (Fig. 21).

Based on the studies carried out, as well as Refs [183, 184], we can conclude the following.

• The main characteristic of an SB in amorphous alloys is *SB power*, which is determined by the height of the step h in the region where the SB emerges on the sample surface divided by the SB thickness t. The power can be related to the value of the true deformation inside the SB using the expression $e_{SB} = \ln(h/t)$.

• Another main characteristic of SBs is their volume density V_{SB}, which, under certain geometrical conditions, can strictly depend on the average distance r between adjacent surface steps: $r \sim V_{SB}^{-1/2}$.

• By analogy with crystals, in amorphous alloys, SBs form slip systems, which are characterized by close values of e_{SB} and r, as well as a certain orientation of the SB surface relative to the principal deformation axes.

• The SB design in bulk amorphous alloys depends mainly on the method of deformation. The magnitude of the total deformation has a decisive effect on the power of the SB. The bulk density of SBs is determined by the nature of the material and the deformation conditions.

• SBs in amorphous alloys, by analogy with dislocations, are capable of carrying out plastic shear in two mutually opposite directions.

• The maximum value of the SB step height, found during HPT, is 2.6–2.9 μm, which corresponds to an SB power equal to $e_{SB} = 4.0-4.2$.

The specificity of SB formation during MPD of amorphous alloys is that already at ordinary macroscopic deformations the power of SB is sufficient for the formation of local MPD zones ($e > 4$) inside the amorphous matrix. In this case, if severe deformations are produced in amorphous

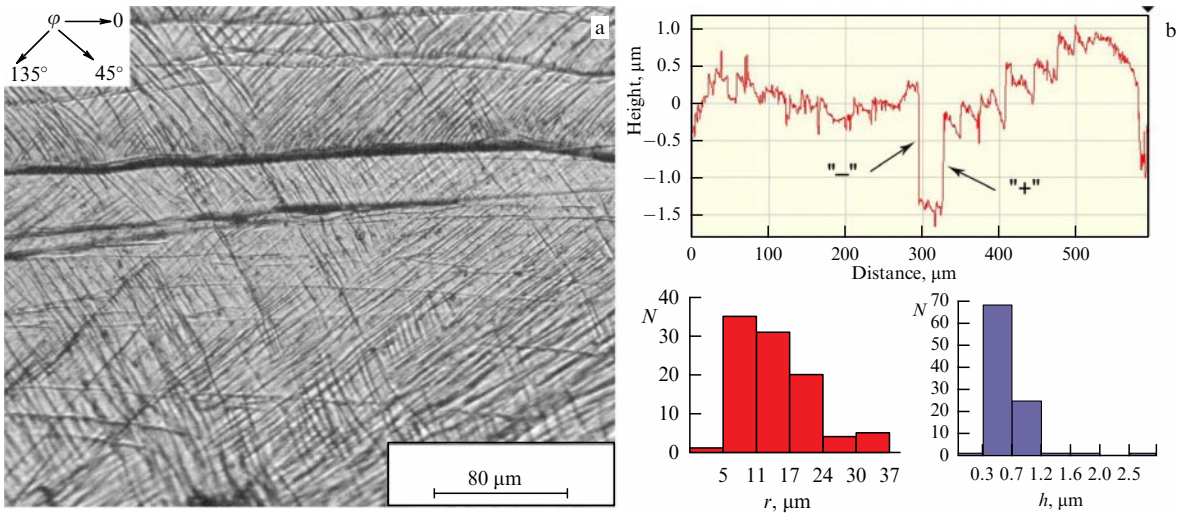

Figure 21. Panoramic picture of SB steps after HPT at room temperature ($n = 1/32$) (a) and corresponding profilogram and histogram of r (red) and h (blue) values (b); arrows indicate SBs with positive (+) and negative (−) shear directions [178].

alloys by HPT, ECAP, etc., then MPD will be observed, as it were, at two structural levels: inside the SB and macroscopically throughout the sample. Consequently, a new variant of plastic deformation is formed — 'megaplastic deformation inside megaplastic deformation,' i.e., in fact, a *gigaplastic* deformation (GPD) of a solid occurs.

As an example, Fig. 22 shows the dependences of the average and most probable value (mode) of the step height h (a) and the average distance between them r (b) for SB steps formed during cold rolling, in comparison with SB steps formed at an increasing value of deformation e for HPT in a Bridgman chamber [178]. There is an obvious tendency for the values of h to increase as e increases (Fig. 22a). However, for the values of r, a tendency toward some decrease (toward an increase in the bulk density of SBs) is observed only for strains in the HPT mode. For samples after rolling at a small deformation ($e = 0.4$), an anomalously high SB density ($r = 2$ μm) was obtained (Fig. 22b). The character of the distribution of the main SB characteristics undergoes certain changes as the value of n increases during HPT. The maximum value h_{max}, which was recorded for the system of steps in Ref. [178], is 2.9 μm ($e_{SB} = 4.0-4.2$).

6.1.2 Effect of fractionality and direction of deformation. One of the factors affecting the structure and properties of materials formed during MPD is the fractionality of deformation, i.e., the number of external action cycles at which the required value of plastic deformation is achieved [108]. In principle, all possible methods of deformation can be conditionally divided into two large groups: continuous and fractional. The number of cycles in the fractional MPD method is not given as much attention as, e.g., temperature or deformation rate. However, the processes of elastic relaxation that occur during a 'pause' between individual passes even at room temperature can significantly affect the defect structure and, consequently, the properties of the material. This is especially true for cases where during external actions the material is subjected to MPD. When using the ECAP method, only a few articles report on the number of passes necessary to achieve the resulting deformation [46]. In Ref. [185], it was theoretically shown that nonmonotonic (in particular, cyclic) loading of a material leads, other things being equal, to less intense grain refinement and a less intense fracture than does the process of quasimonotonic loading.

In Ref. [186], an attempt was made to evaluate experimentally the 'fractionality effect' in MPD. To produce severe deformations, a Bridgman chamber was used, in which HPT was implemented. Commercially pure iron was chosen as the material for the study. The experiments were carried out as follows (Fig. 23). The total deformation of the sample in all cases corresponded to two full revolutions of the movable

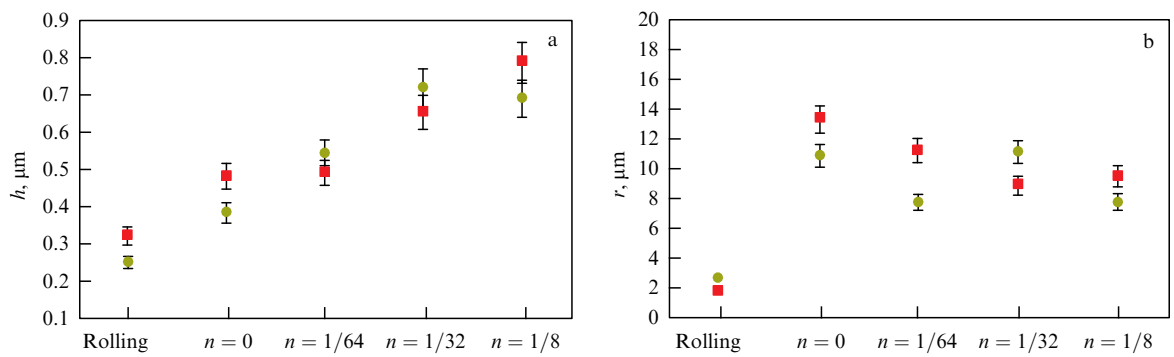

Figure 22. Dependences of mean values (squares) and mode values (dots) for parameters h (a) and r (b) of SB in the case of rolling and HPT (for different values of n) [178].

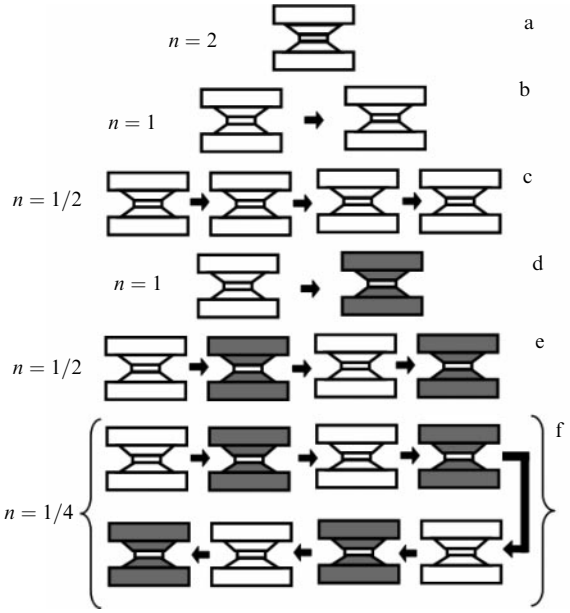

Figure 23. Schematic diagram of experiments: (a) continuous deformation; (b–d) deformation of the '→' type with a different number of fractional deformation cycles; (e, f) deformation of the '↔' type with a different number of fractional deformation cycles; n is the number of revolutions in one fractional cycle of deformation. White and gray indicate the rotation of the lower anvil in the forward and reverse directions, respectively [186].

anvil ($N = 2$) and amounted to $e_N = 6.2$. The deformation was carried out according to several options (see Fig. 23). Option (a) was a continuous deformation in one partial pass n, equal to two full revolutions of the movable anvil ($N = 2$, $n = 2$). In the case of option (b), the sample was subjected to deformation in two passes in one direction of rotation of the movable anvil (→), each partial pass n being one full revolution ($N = 2, \rightarrow, n = 1$). Option (c) corresponded to four partial passages in one direction of rotation of the movable anvil ($N = 2, \rightarrow, n = 1/2$). Options (d) and (e) were similar to options (b) and (c), respectively, with the only difference being that the rotation directions alternated (↔). For deformation with alternately changed direction of the movable anvil rotation, option (f) was implemented with an even greater number of partial passages ($N = 2, \leftrightarrow, n = 1/4$).

Figure 24a, b shows the dependence of the proportion of recrystallized grains C_{RG} and the proportion of deformation fragments C_{DF} on the number of partial cycles n for deformation experiments of the '→' type (torsion in the same direction in each cycle) and the '↔' type (torsion with alternately changing direction in every subsequent cycle). It can be seen that for the '→' option, the MPD 'fractionality effect' leads to a noticeable decrease in C_{RG} (up to 0.25 at $n = 1/2$) and to a corresponding increase in C_{DF} to 0.75, whereas, after continuous deformation ($n = 2$), they were practically equal ($C_{RG} = C_{DF} = 0.5$). In the case of '↔' deformation experiments, this 'fractionality effect' is completely different: the value of C_{RG} tends to some increase with saturation at small values of n ($C_{RG} \rightarrow 0.65$), and the value of C_{DF} tends to decrease with saturation at small values n ($C_{DF} \rightarrow 0.35$).

Figures 24c, d present the dependences of the mean size of deformation fragments D_{DF} and recrystallization grains D_{RG} on n for the type '→' (c) and type '↔' (d) experiments. The dependences $D(n)$ for both loading options are symbate in nature: the average DF and RG dimensions have a characteristic minimum at $n = 1$, increasing (to a greater extent for '→') as the value of n decreases or increases.

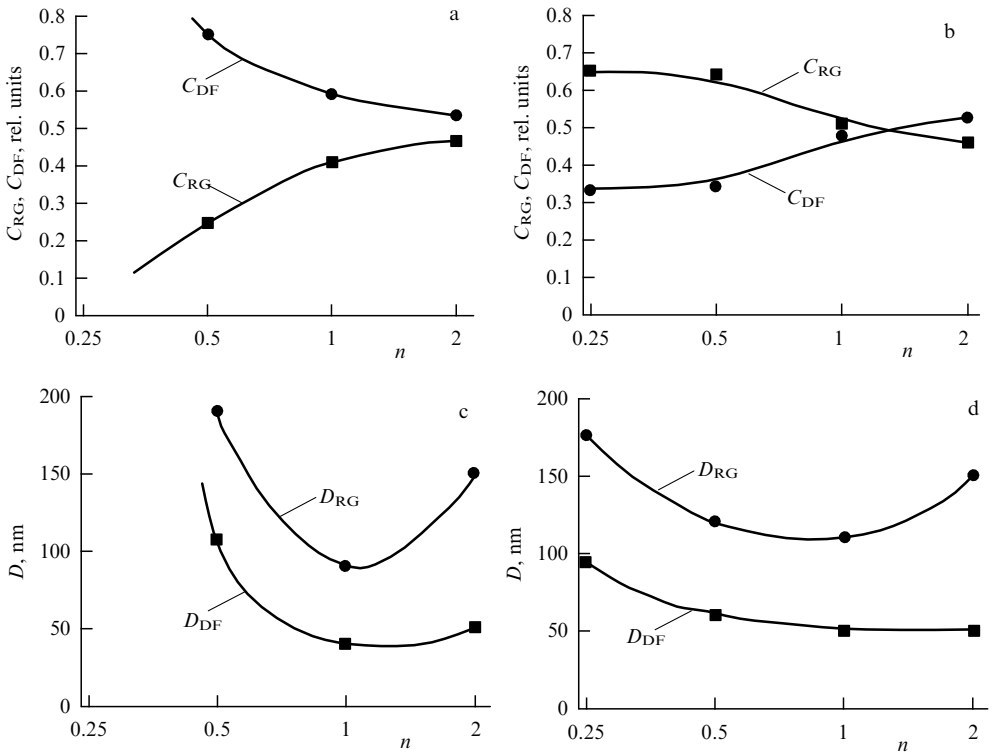

Figure 24. Relative volume fraction of recrystallized grains (C_{RG}) and deformation fragments (C_{DF}) depending on the value of fractional deformation n of the type '→' (a) and '↔' (b), as well as mean sizes of recrystallized grains (D_{RG}) and deformation fragments (D_{DF}) depending on the value of fractional deformation n of the type '→' (c) and '↔' (d) [186].

The experiments carried out have shown that the cyclicity of the external load application has a noticeable effect on the deformation behavior (structure and mechanical properties of metals) subjected to MPD. This gives grounds to believe that, for a correct description of the deformation methods used, it is necessary to indicate the number of cycles of applying an external load and the amount of plastic deformation in each of them (for example, in titanium alloys [172]). It can also be assumed that, due to the generality of the processes occurring under severe deformations, conclusions about the significance of the 'fractionality effect' are valid not only for HPT but also for ECAP, twist extrusion, accumulative rolling, volumetric forging, and other methods of MPD in metallic materials.

6.2 Accompanying processes

The most characteristic phenomena accompanying MPD, but directly creating no effects of plastic deformation, are the processes of redistribution of the phase and chemical composition on the scale of the deformed sample. A number of review articles have been devoted to these processes, including the formation of mass transfer vortices [187], diffusion phase transformations [188, 189], and grain-boundary segregations [190].

6.2.1 Ordering and disordering of solid solutions. Plastic deformation, by creating point defects and increasing the bulk density of shear antiphase boundaries (SAPBs), violates the long-range order in ordered solid solutions. The most complete information on the disappearance of the ordered state as a result of deformation processes has been obtained for the superstructures Ni_3Al [191, 192], Al_3Ti [193, 194], Fe_3Al [192, 194], FeAl [193, 195], Cu_3Au [196], Nb_3Au, and V_3Ga [197]. Restoration of the long-range order during deformation at room and lower temperatures was hardly observed. Only in Ref. [198], at elevated temperatures, was a local increase in the degree of long-range order detected in the ordered Ni_3Fe alloy within a narrow range of rolling deformation degrees. Restoration of ordering after its complete suppression during deformation has never been observed.

The literature very sparingly reflects the features of the behavior of ordered alloys and, in particular, the nature of the change in the long-range order degree during MPD. Of recent studies, worth noting is only Ref. [199], in which the change in the degree of long-range order in the FeCo superstructure ordered according to the B2 type and in the Ni_3Fe superstructure ordered according to the $L1_2$ type was studied after MPD at room temperature under HPT in the Bridgman chamber. It was found that the long-range order in the studied alloys was completely destroyed at $n \geqslant 1/2$ in the Ni_3Fe alloy and at $n \geqslant 1$ in the FeCo alloy (n being the MPD measure equal to the number of complete revolutions of the Bridgman movable anvil).

Are there fundamental differences in the nature of the change in the degree of long-range order in superstructures under the influence of ordinary deformations and MPD in the region of relatively low temperatures? Reference [200] was devoted to solving this problem, where the behavior of long-range $D0_3$ order parameters was studied in the Fe – 24 at.% Al alloy, the composition of which is close to the stoichiometric composition A_3B, after deformation treatments by HPT at room temperature in a Bridgman chamber.

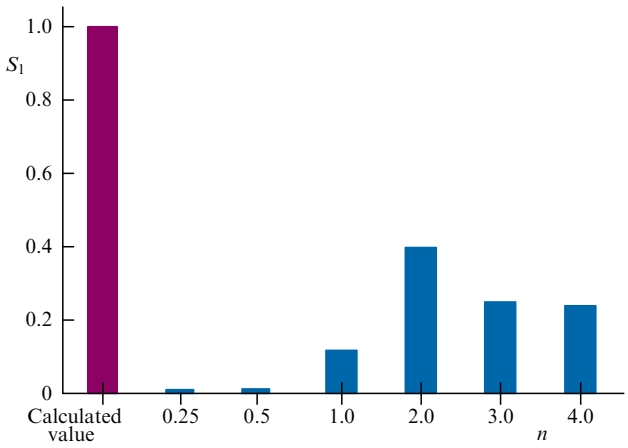

Figure 25. Dependence of long-range order parameter S_1 on the value n of HPT deformation at room temperature of the initially ordered alloy Fe – 24 at.% Al [200].

In Ref. [200], a new previously unknown phenomenon was discovered: as a result of MPD at room temperature, the Fe_3Al superstructure first undergoes almost complete suppression of the long-range order, and then its partial restoration (Fig. 25). Undoubtedly, the observed effect is associated with the peculiarities of the structural transformations during MPD. It was found that, at the initial stages of MPD ($n < 1$) in the ordered structure, defects (dislocations and SAPBs [201]) accumulate, reducing the effective parameters of the long-range order. In local areas of deformation fragments with a high concentration of defects and internal stresses, a critical state is reached, in which atomic disordering occurs or only short-range order is preserved in the structure. At $n \geqslant 1$, an additional channel for the dissipation of mechanical energy introduced during MPD appears in the material, i.e., continuous dynamic recrystallization [71], which is undoubtedly associated with a local increase in temperature and, accordingly, with an anomalously high atomic mobility at low temperatures [202]. In the resulting recrystallized grains, conditions are created for the restoration of long-range order. As n increases, the proportion of recrystallized grains increases and, accordingly, increases the degree of long-range order averaged over the crystal.

At high deformations ($n \geqslant 2$), a steady two-phase state arises in the deformed system under MPD conditions, in which $K = V_{RG}/V_{DF} = \text{const}$, where V_{RG} and V_{DF} are the volume fractions of RGs and DFs, respectively. Depending on the material nature and the conditions for MPD implementation, the value of K can vary within 0.4–0.6. It was found that the deformation conditions during MPD ensure almost complete restoration of the long-range order in the first coordination sphere and partial restoration of the long-range order in the second coordination sphere.

To explain the above features, let us turn to the phase diagram of the Fe – Al system [203] (Fig. 26). The local increase in temperature during MPD could reach 500–550 °C, at which the alloy of the composition studied by us turned out to be in the process of dynamic recrystallization in the two-phase region of the state diagram (B2 + A2) (miscibility gap). Furthermore, during suspension of the HPT process, a fast decrease in temperature occurs, fixing the high-temperature ordered state of the system.

It is important to emphasize that MPD is, undoubtedly, an open system that obeys the laws of nonequilibrium

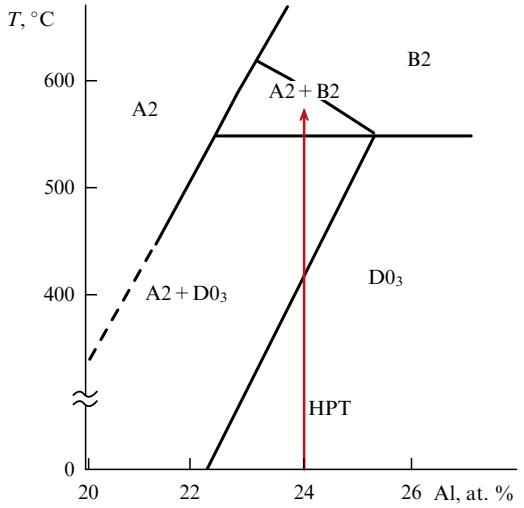

Figure 26. Part of the state diagram of the Fe–Al system [203], which demonstrates the shift of the equilibrium state from the $D0_3$ superstructure to (A2 + B2) during a short-term increase in temperature under the action of HPT at room temperature; A2 — disordered FeAl phase [200].

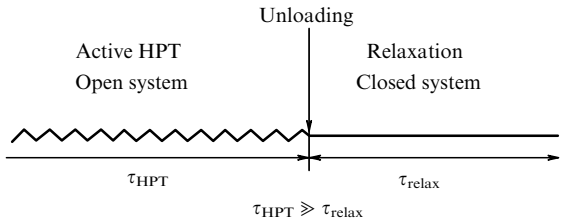

Figure 27. Schematic diagram of two stages of the HPT process: the first one is the MPD process, the second is the relaxation process after removing the external load [200].

thermodynamics, and, therefore, the emerging structural phase states cannot be correctly described using state diagrams obtained in the framework of equilibrium thermodynamics. However, in a number of studies, the authors ignore such a contradiction and actively use state diagrams to analyze phases formed during MPD, e.g., when considering a change in the nature of ordering in the Fe–24 at.% Al alloy during HPT [200].

The contradiction we are discussing can be resolved by considered HPT as a two-stage process (Fig. 27). The first stage is the actual deformation in the MPD regime with the dominant role of nonequilibrium thermodynamics leading, in particular, to the formation of a stationary state under conditions of dynamic recrystallization. At the second stage (the stage of unloading), the deformation is suspended and the system relaxes in accordance with the laws inherent in a closed system. The relaxation stage takes place over a very short period of time (apparently, microseconds [140]). However, if the temperature is sufficiently high (in our case above 500 °C), then a limited relaxation time may be quite sufficient for processes characterized by high rates and small diffusion paths to proceed. It is these processes to which atomic ordering can be attributed, whose implementation requires the movement of atoms within one unit cell. Each of these processes requires a certain relaxation time, which, under certain temperature conditions, should be less than

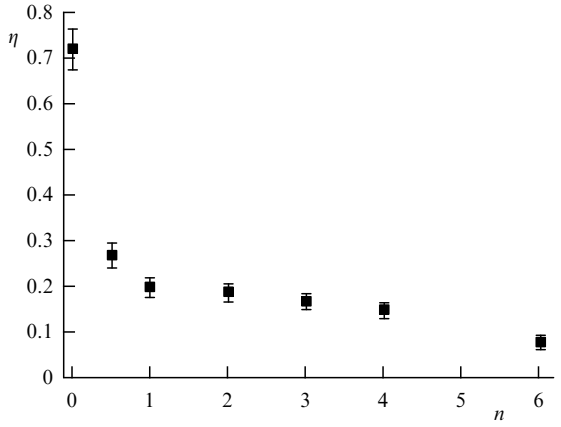

Figure 28. Influence of the HPT value (n) at room temperature on the degree of long-range B2-type order (η), found in the FeCo alloy using the thermal neutron diffraction technique [204].

the critical structural relaxation time determined by the MPD conditions and the nature of the material.

Similar studies in the B2-ordered FeCo alloy showed even more unexpected results [204]. In this study, using diffraction of thermal neutrons and EXAFS spectroscopy, we studied the features of the atomic ordering process and the structural and magnetic characteristics that depend on it in an alloy under HPT at room and higher temperatures of deformation and subsequent annealing. The thermal neutron diffraction method (wavelength $\lambda = 1.675$ Å) based on the IR-8 reactor at the National Research Center, Kurchatov Institute, was used to determine the degree of long-range atomic B2-type ordering after various values of HPT. EXAFS spectra above the K-absorption edges of Co and Fe were measured at the experimental Structural Materials Science station of the synchrotron radiation source Sibir-2 of the Kurchatov Institute in the transmission mode at room temperature. A sharp decrease in the degree of long-range order with increasing HPT (Fig. 28) was found to be in correspondence with EXAFS spectroscopy data, from which it follows that almost perfect B2-type ordering is retained in the nearest coordination spheres of Fe and Co atoms (Fig. 29, Tables 1 and 2). The results obtained demonstrate some contradictions: the retention of an almost ideal B2-type long-range order in the nearest coordination spheres of Fe and Co atoms, regardless of the HPT value (EXAFS spectroscopy) but, at the same time, a sharp decrease in the degree of B2-type long-range order with increasing HPT deformations (neutron diffraction).

In Ref. [204], the authors revealed that the discovered contradictions are only seemingly so. This conclusion is based on the following. The dissipative thermal energy arising during HPT in both Fe–Al and Fe–Co alloys can lead to a short-term increase in the temperature of a deformed solid, which results in the formation of ordered structure regions [200]. In the Fe–Al system, the ordering energy of the solid solution and the diffusion mobility of atoms are so high that atomic B2-type ordering has time to be implemented in a significant way. In the Fe–Co alloy, at significant ordering energies in the first and second coordination spheres ($(500 \pm 160)k$ and $(0 \pm 120)k$, respectively, where $k = 13.8 \times 10^{-24}$ J [205]), the phase transition A2 (bcc disordered solid solution) $\rightarrow$ B2 has time to proceed to a much lesser extent than in Fe–Al alloys, because Fe–Co

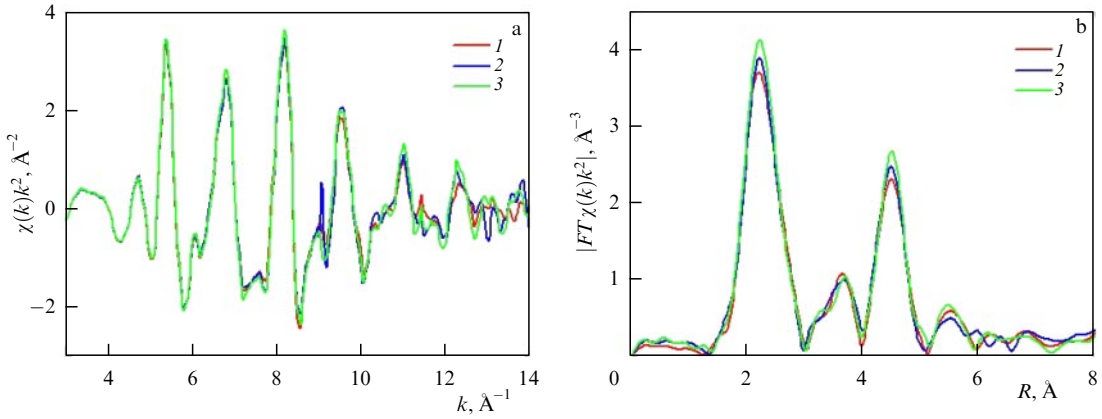

Figure 29. Experimental EXAFS functions (a) measured above the *K*-edge of Co, as well as the corresponding Fourier transform moduli of experimental EXAFS functions (b) for FeCo alloy samples; *1* — initial state before HPT, *2* — HPT at $n = 1$, *3* — HPT at $n = 4$. HPT is performed at room temperature [204].

Table 1. Results of calculations of the influence of HPT on the type of nearest neighbors of Fe atoms in the FeCo alloy.

Initial state			
	$N_n \pm 0.5$	$R \pm 0.01$, Å	$\sigma^2 \pm 0.001$, Å^{-1}
Fe–Fe	1	2.16	0.007
Fe–Co	7	2.42	0.010
Fe–Fe	6	2.79	0.007
HPT ($n = 1$)			
Fe–Fe	1	2.16	0.008
Fe–Co	7	2.42	0.010
Fe–Fe	4	2.85	0.006
HPT ($n = 4$)			
Fe–Fe	1.5	2.19	0.012
Fe–Co	6.5	2.42	0.009
Fe–Fe	6	2.79	0.007

Table 2. Results of calculations of the influence of HPT on the type of nearest neighbors of Co atoms in the FeCo alloy.

Initial state			
	$N_n \pm 0.5$	$R \pm 0.01$, Å	$\sigma^2 \pm 0.001$, Å^{-1}
Co–Co	1	2.15	0.008
Co–Fe	7	2.46	0.009
Co–Co	4	2.85	0.006
Co–Fe	2	2.72	0.004
HPT ($n = 1$)			
Co–Co	1	2.18	0.017
Co–Fe	7	2.47	0.008
Co–Co	4	2.85	0.006
Co–Fe	2	2.69	0.002
HPT ($n = 4$)			
Co–Co	1	2.18	0.011
Co–Fe	7	2.47	0.008
Co–Co	5	2.85	0.009
Co–Fe	1	2.72	0.001

alloys at the same temperatures have significantly lower self-diffusion coefficients [206, 207]. As a result, the long-range order in the studied Fe–Co alloy is realized during HPT in the form of ultradispersed domains including only a few coordination spheres. Such domains are not capable of forming superstructure lines in neutron diffraction patterns, but form EXAFS spectra corresponding to a high degree of B2-type atomic order in the nearest coordination spheres of Fe and Co atoms. Thus, HPT deformation at room temperature in the Fe–Co alloy suppresses long-range B2-type order ($\eta \to 0$) but retains a high degree of local B2-type ordering in the nearest coordination spheres. The absence of decrease in the saturation magnetization σ with increasing n (see Fig. 7), in fact, means that, in full accordance with modern theoretical concepts [208], it is the exchange interaction of Fe and Co atoms in the nearest coordination spheres that determines ferromagnetic characteristics of the alloy.

6.2.2 Redistribution of components in composite materials. One of the most significant accompanying processes that do not create deformation effects is the change in local concentrations of components in chemically inhomogeneous materials under the influence of MPD. In this connection, of great interest is the behavior during MPD of composite materials consisting of several structural components that differ significantly in their chemical composition or have limited mutual solubility [209]. The atomic mechanisms of redistribution of components at low temperatures during MPD are debatable. Most often, they are associated either with direct mixing of atoms, which does not cause dislocation-like shifts [210], or with processes close in nature to the Gleiter mechanism [211] (interaction of moving dislocations with migrating impurity atoms).

In the course of interaction among the atomic constituents of the composite, which are limitedly soluble or even completely mutually insoluble at equilibrium, various processes can occur during MPD [212]: the formation of supersaturated solid solutions based on one of the components (e.g., in the Cu–Nb system [213]), the formation of amorphous phases with variable composition (e.g., in the

same Cu – Nb system [214]), or the formation of new phases at the interfaces, which noticeably strengthen the composite material (e.g., nanoparticles of the Al_2Cu phase in the Al – Cu system [215] or AlTi, Al_3Ti, and $AlTi_3$ phases in the Al – Ti system [216]). In the last case, strengthening nanoparticles were found in the transitional boundary zone of two Al and Cu ribbon samples deformed in a Bridgman chamber by five revolutions at room temperature and a hydrostatic pressure of 5 GPa.

In Ref. [217], composites consisting of freely stacked alternating ribbons of two amorphous alloys based on iron and cobalt were subjected to joint HPT treatment. Using the method of electron mass spectrometry, three stages of evolution of the structural phase state of the formed composites were established as the amount of HPT deformation increased. At the first stage, the structural components of the composite are deformed quite independently of each other, providing only mechanical adhesion of adjacent layers. At the second stage of HPT, interfacial interaction of thin near-boundary regions occurs with the effects of vortex mixing and with the formation of boride strengthening phases. At the final, third stage of HPT, the transported vortex flows of matter interact up to complete mixing and formation of a homogeneous multicomponent alloy, which is in fact equivalent to the 'disappearance' of the original composite.

7. Conclusion

(1) MPD is a structurally determined, independent, and specific stage of plastic deformation inherent in all solids, regardless of the stress state organization. It is realized according to special structural mechanisms, including dislocation, disclination, grain-boundary and other modes of active plastic flow in combination with structural rearrangements of a relaxation and dissipative nature.

(2) Regularities of MTD are entirely based on the postulates of nonequilibrium thermodynamics. A deformable solid body should be considered a mechanical dissipative system, in which the total energy is continuously reduced or dissipated, converting into other, non-mechanical forms of energy (chemical, electromagnetic, thermal, etc.). Within the framework of nonequilibrium evolutionary thermodynamics (NET), it is possible to describe from a unified standpoint the change in the defect structure of polycrystalline and amorphous metallic materials in the course of MPD. By explicitly taking into account the main channels of dissipation, generation, and annihilation of defects, the main relation of thermodynamics (the Gibbs relation) is generalized to the case of a strongly nonequilibrium MPD process. A common feature of all processes during MPD is the existence of a stationary state naturally described within the framework of the NET formalism.

(3) Structural processes that occur during MPD can be conditionally divided into two independent (or weakly coupled) groups: processes directly responsible for the implementation of plastic flow, and accompanying processes that have only an indirect effect on plastic deformation. MPD, as a rule, includes a stage of developed plastic deformation, when deformation fragmentation processes actively occur with the formation of relatively defect-free regions separated by boundaries with a wide range of crystallographic misorientations, including small, medium, and large angular values.

(4) For the reconstruction of the defect structure in the process of MPD, plastic deformation is 'vitally' necessary. It plays the role of a fundamental drive, with the help of which a new type of equilibrium state is formed — a limiting or stationary structure. Thermal motion in MPD processes plays a secondary, subordinate role. It is important only for the processes of 'soft' relaxation after the completion of MPD, when the system 'eliminates' deviations from classical thermodynamic equilibrium with the help of atomic diffusion.

(5) Under ordinary (macroplastic) deformations, a gradual accumulation of elastic energy (strain hardening) takes place, and only at the stage of MPD do powerful accommodative and dissipative processes 'switch on.' Additional effective channels for relaxation of mechanical energy are dislocation-disclination accommodation, dynamic recrystallization, and phase transformations (including the transition to an amorphous state). The flow of mechanical energy supplied to the solid body is completely converted into thermal energy as the system proceeds to the stationary MPD mode. In this regard, the statements of some authors that there are no processes of latent heat release with a deformation origin and no corresponding effects of a local and short-term increase in temperature [90] seem not to be quite correct.

(6) Taking into account two types of main structural defects (dislocations and grain boundaries), for polycrystals, a unified hardening curve is theoretically and experimentally obtained, which is approximated by the Hall–Petch law at the initial stage of MPD, and then at the main, most intensive stage of the process, by the linear hardening law. The transition of the system to a stationary regime for both types of defects leads to the complete absence of strain hardening effects.

(7) The fragmentation phenomenon is the main result of the dislocation-disclination accommodation process and can be described by the model proposed by V V Rybin [45] with the attraction of the dynamic recrystallization model [50]. The attempt by the authors of Ref. [38] to artificially divide the process of giant plastic deformations into 'intense plastic deformations' (fragmentation is present) and 'large plastic deformations' (fragmentation is absent) is erroneous and not only does not clarify, but, on the contrary, complicates even more the understanding of physical processes that occur upon significant deformations, and creates considerable confusion. For example, it follows from Ref. [38] that plastic deformation by rolling should be attributed to 'large plastic deformations,' although it is well known [45] that obvious signs of fragmentation are observed during cold rolling of polycrystals of bcc metals.

(8) It is important to note the cyclical nature of the processes during MPD. Competition between the creation and annihilation of defects occurs with a different rate at different stages. At the initial stage, the predominating processes are those of generating structural defects or new phases and, at later stages, their annihilation. Depending on the characteristics of the defects and the current state of the system, the stationary regime can be reached either monotonically or via damped oscillations.

(9) The specific scenario of structural transformations during MPD is determined by their ability to effectively compensate for the increase in the internal energy of an open system. It depends on a number of factors (the temperature, the value of the Peierls barrier of dislocations

and their ability to undergo diffusion rearrangements, the difference between the free energies of nonequilibrium and equilibrium crystalline and amorphous phases).

(10) MPD does not at all guarantee the formation of a nanocrystalline state with a crystallite size of less than 100 nm, separated by high-angle or interphase boundaries. For example, in pure metals with high dislocation mobility, this is practically impossible. An important factor in the formation of nanostructures during MPD is the occurrence of martensitic and diffusion phase transformations, as well as the transition to an amorphous state. By stimulating phase transformations by varying the temperature and chemical composition of materials, we can obtain nanostructures of various types.

(11) It is possible to determine with rather high accuracy the critical deformation region where macroplastic deformation transforms into an MPD. The boundary region of MPD implementation is distinctly determined by the beginning of activation of one of the possible additional dissipation channels. Morphologically, the MPD stage can be detected, for example, by the appearance of dynamically recrystallized grains or amorphous phase microscopic regions in the structure.

The study was carried out within the framework of the state task of the Ministry of Education and Science of the Russian Federation (project code 0718-2020-0037) and was supported by the Russian Science Foundation (project no. 19-72-20066) and Russian Foundation for Basic Research (project no. 20-12-50035 Ekspansia).

References

1. Fortov V E *Ekstremal'nye Sostoyaniya Veshchestva* (Extreme States of Matter) (Moscow: Fizmatlit, 2009)
2. Fortov V E *Phys. Usp.* **50** 333 (2007); *Usp. Fiz. Nauk* **177** 347 (2007)
3. Kanel' G I, Fortov V E, Razorenov S V *Phys. Usp.* **50** 771 (2007); *Usp. Fiz. Nauk* **177** 809 (2007)
4. Fortov V E *Phys. Usp.* **52** 615 (2009); *Usp. Fiz. Nauk* **179** 653 (2009)
5. Kanel' G I, Zaretskii E B, Razorenov S V, Ashitkov S I, Fortov V E *Phys. Usp.* **60** 490 (2017); *Usp. Fiz. Nauk* **187** 525 (2017)
6. Fortov V E, Lomonosov I V *Phys. Usp.* **57** 219 (2014); *Usp. Fiz. Nauk* **184** 231 (2014)
7. Glezer A M et al. *Plastic Deformation of Nanostructured Materials* (Boca Raton, FL: Taylor and Francis Group, 2017); Translated from Russian: *Osnovy Plasticheskoi Deformatsii Nanostrukturnykh Materialov* (Moscow: Fizmatlit, 2016)
8. Beygelzimer Y et al. *Adv. Mater.* **33** 2005473 (2021)
9. Bridgman P W *Studies in Large Plastic Flow and Fracture, with Special Emphasis on the Effects of Hydrostatic Pressure* (Cambridge, MA: Harvard Univ. Press, 1964); Translated into Russian: *Issledovaniya Bol'shikh Plasticheskikh Deformatsii i Razryva: Vliyanie Vysokogo Gidrostaticheskogo Davleniya na Mekhanicheskie Svoistva Materialov* (Moscow: Librokom, 2010)
10. Rakovskii A V *Usp. Fiz. Nauk* **1** 39 (1918) https://doi.org/10.3367/UFNr.0001.191801d.0039
11. Bridgman P W *Rev. Mod. Phys.* **7** 1 (1935); *Usp. Fiz. Nauk* **16** 64 (1936)
12. Bridgman P W *Trans. Am. Inst. Met. Eng.* **128** 15 (1938); *Usp. Fiz. Nauk* **20** 513 (1938)
13. Bridgman P W *Am. Scientist* **31** (1) 1 (1943); *Usp. Fiz. Nauk* **29** 305 (1946)
14. Bridgman P W *Rev. Mod. Phys.* **18** 1 (1946) pp. 1–27; *Usp. Fiz. Nauk* **31** 53 (1947)
15. Bridgman P W *Rev. Mod. Phys.* **18** 1 (1946) pp. 27–59; *Usp. Fiz. Nauk* **31** 210 (1947)
16. Bridgman P W *Rev. Mod. Phys.* **18** 1 (1946) pp. 59–93; *Usp. Fiz. Nauk* **31** 346 (1947)
17. Zhilyaev A P, Langdon T G *Prog. Mater. Sci.* **53** 893 (2008)
18. Beresnev B I *Some Problems of Large Plastic Deformation of Metals at High Pressures* (Oxford: Pergamon Press, 1963); Translated from Russian: *Nekotorye Voprosy Bol'shikh Plasticheskikh Deformatsii Metallov pri Vysokikh Davleniyakh* (Moscow: Izd. AN SSSR, 1960)
19. Zhorin V A, Livshits L D, Enikolopyan N S *Dokl. Akad. Nauk SSSR* **258** 110 (1981)
20. Segal V M *Mater. Sci. Eng. A* **271** 322 (1999)
21. Valiev R Z, Islamgaliev R K, Alexandrov I V *Prog. Mater Sci.* **45** 103 (2000)
22. Glezer A M, Metlov L S *Phys. Solid State* **52** 1162 (2010); *Fiz. Tverd. Tela* **52** 1090 (2010)
23. Glezer A M, Sundeev R V *Mater. Lett.* **139** 455 (2015)
24. Razumov I K, Gornostyrev Yu N, Ermakov A E *Phys. Met. Metallogr.* **119** 1133 (2018); *Fiz. Met. Metalloved.* **119** 1195 (2018)
25. Dudarev E F *Mikroplasticheskaya Deformatsiya i Predel Tekuchesti Polikristallov* (Microplastic Deformation and Yield Strength of Polycrystals) (Tomsk: Tomsk. Univ., 1988)
26. McMahon C J (Jr.) (Ed.) *Microplasticity* (Advances in Materials Research, Vol. 2) (New York: Interscience, 1968); Translated into Russian: Geminov V N, Rakhshtadt A G (Eds) *Mikroplastichnost'* (Collection of Articles, translation from English E K Zakharov) (Moscow: Metallurgiya, 1972)
27. Stremel' M A *Prochnost' Splavov* (Strength of Alloys) Pt. 2 (Moscow: MISiS, 1997)
28. Golovin Yu I *Universal'nye Printsipy Estestvoznaniya* (Universal Principles of Natural Science) (Tambov: Tambov. Gos. Univ., 2002)
29. Metlov L S *Metallofiz. Noveish. Tekhnol.* **29** 335 (2007)
30. Metlov L S *Phys. Rev. E* **90** 022124 (2014)
31. Pérez-Reche F-J, Truskinovsky L, Zanzotto G *Phys. Rev. Lett.* **99** 075501 (2007)
32. Metlov L S *Phys. Rev. E* **81** 051121 (2010)
33. Glezer A M *Bull. Russ. Acad. Sci. Phys.* **71** 1722 (2007); *Izv. Ross. Akad. Nauk Ser. Fiz.* **71** 1764 (2007)
34. Pozdnyakov V A, Glezer A M *Bull. Russ. Acad. Sci. Phys.* **68** 1621 (2004); *Izv. Ross. Akad. Nauk Ser. Fiz.* **68** 1449 (2004)
35. Metlov L S *Neravnovesnaya Evolyutsionnaya Termodinamika i Ee Prilozheniya* (Non-Equilibrium Evolutionary Thermodynamics and Its Applications) (Donetsk: Noulidzh. Donets. Otd., 2014)
36. Glezer A M et al. *Mater. Sci. Forum* **584–586** 227 (2008)
37. Metlov L S *Bull. Russ. Acad. Sci. Phys.* **72** 1283 (2008); *Izv. Ross. Akad. Nauk Ser. Fiz.* **72** 1353 (2008)
38. Utyashev F Z, Beygelzimer Y E, Valiev R Z *Adv. Eng. Mater.* **23** 2100110 (2021)
39. Utyashev F Z, Raab G I *Deformatsionnye Metody Polucheniya i Obrabotki Ul'tramelkozernistykh i Nanostrukturnykh Materialov* (Deformation Methods for Obtaining and Processing Ultrafine-Grained and Nanostructured Materials) (Ufa: Gilem, 2013)
40. Utyashev F Z et al. *Russ. Metallurgy* (*Metally*) **2019** (4) 281 (2019); Translated from Russian: *Deformatsiya Razrushenie Mater.* (10) 2 (2018)
41. Segal V *Metals* **10** 244 (2020)
42. Segal V *Mater. Sci. Eng. A* **338** 331 (2002)
43. Valiev R Z, Langdon T G *Prog. Mater. Sci.* **52** 881 (2006)
44. Bridgman P W *J. Appl. Phys.* **17** 692 (1946)
45. Rybin V V *Bol'shie Plasticheskie Deformatsii i Razrushenie Metallov* (Large Plastic Deformations and Fracture of Metals) (Moscow: Metallurgiya, 1986)
46. Estrin Y, Vinogradov A *Acta Mater.* **61** 782 (2013)
47. Vinogradov A, Estrin Y *Prog. Mater Sci.* **95** 172 (2018)
48. Svirina Yu V, Perevezentsev V N *Russ. Metallurgy* (*Metally*) **10** 807 (2014); Translated from Russian: *Deformatsiya Razrushenie Mater.* (7) 2 (2013)
49. Glezer A M et al. *Dokl. Phys.* **59** 360 (2014); *Dokl. Ross. Akad. Nauk* **457** 535 (2014)
50. Glezer A M, Tomchuk A A *Rev. Adv. Mater. Sci.* **45** 9 (2016)
51. Kopylov V I, Chuvil'deev V N, in *Severe Plastic Deformation* (Ed. A Burhanettin) (New York: Nova Science Publ., 2006)
52. Chuvil'deev V N et al. *Dokl. Phys.* **49** 296 (2014); *Dokl. Ross. Akad. Nauk* **396** 332 (2004)
53. Chuvil'deev V N *Neravnovesnye Granitsy Zeren v Metallakh. Teoriya i Prilozheniya* (Non-Equilibrium Grain Boundaries in Metals. Theory and Applications) (Moscow: Fizmatlit, 2004)

54. Malygin G A *Phys. Usp.* **42** 887 (1999); *Usp. Fiz. Nauk* **169** 979 (1999)
55. Malygin G A *Phys. Solid State* **44** 1305 (2002); *Fiz. Tverd. Tela* **44** 1979 (2002)
56. Panin V E et al. *Sov. Phys. J.* **30** 24 (1987); *Izv. Vyssh. Uchebn. Zaved. Fiz.* **30** 34 (1987)
57. Bazarov I P *Thermodynamics* (Oxford: Pergamon Press, 1964); Translated from Russian: *Termodinamika* (Moscow: Vysshaya Shkola, 1991)
58. Metlov L S *Phys. Rev. Lett.* **106** 165506 (2011)
59. Olemskoi A I, Khomenko A V *J. Exp. Theor. Phys.* **83** 1180 (1996); *Zh. Eksp. Teor. Fiz.* **110** 2144 (1996)
60. Khomenko A V, Lyashenko I A *Phys. Usp.* **55** 1008 (2012); *Usp. Fiz. Nauk* **182** 1081 (2012)
61. Prokof'eva O V et al. *Russ. Metallurgy* (*Metally*) **2017** (3) 226 (2017); Translated from Russian: *Deformatsiya Razrushenie Mater.* (2) 76 (2017)
62. Rubi J M, Gadomski A *Physica A* **326** 333 (2003)
63. Metlov L S *Fiz. Tekh. Vys. Davl.* **29** (1) 28 (2019)
64. Khomenko A V, Troshchenko D S, Metlov L S *Metallofiz. Noveish. Tekhnol.* **39** (2) 265 (2017)
65. Firstov S A et al. *Rev. Adv. Mater. Sci.* **4** 155 (2003)
66. Pechina E A et al. *Russ. Metallurgy* (*Metally*) **2014** (10) 846 (2014); Translated from Russian: *Deformatsiya Razrushenie Mater.* **4** (4) 41 (2013)
67. Metlov L S *Deformatsiya Razrushenie Mater.* (2) 40 (2007)
68. Metlov L S, Glezer A M, Varyukhin V N *Russ. Metallurgy* (*Metally*) **2015** (4) 269 (2015); Translated from Russian: *Deformatsiya Razrushenie Mater.* (5) 8 (2014)
69. Sakai T, Miura H, Yang X *Mater. Sci. Eng. A* **499** 2 (2005)
70. Glezer A M *Phys. Usp.* **55** 522 (2012); *Usp. Fiz. Nauk* **182** 559 (2012)
71. Sakai T et al. *Acta Mater.* **57** 153 (2009)
72. Humphreys F J, Hatherly M *Recrystallization and Related Annealing Phenomena* (Amsterdam: Elsevier, 2004)
73. Kassner M E, Barrabes S R *Mater. Sci. Eng. A* **410–411** 152 (2005)
74. Andrievskiy R A, Glezer A M *Phys. Usp.* **52** 315 (2009); *Usp. Fiz. Nauk* **179** 337 (2009)
75. Gutkin M Y, Ovid'ko I A *Plastic Deformation of Nanocrystalline Materials* (Berlin: Springer, 2004)
76. Glezer A M et al. *Mater. Lett.* **161** 360 (2015)
77. Glezer A M et al. *Bull. Russ. Acad. Sci. Phys.* **78** 1155 (2014); *Izv. Ross. Akad. Nauk Ser. Fiz.* **78** 1273 (2014)
78. Blinova E N et al. *Materialovedenie* (5) 32 (2005)
79. Nalimov V V *Teoriya Eksperimenta* (Theory of Experiment) (Moscow: Nauka, 1974)
80. Gorelik S S et al. *Rekristallizatsiya Metallov i Splavov* (Recrystallization of Metals and Alloys) (Moscow: MISiS, 2005)
81. Schwartz A et al. (Eds) *Electron Backscatter Diffraction in Materials Science* (New York: Springer, 2009)
82. Glezer A M et al. *Tech. Phys. Lett.* **43** 399 (2017); *Pis'ma Zh. Tekh. Fiz.* **43** (8) 79 (2017)
83. Glezer A M et al. *Bull. Russ. Acad. Sci. Phys.* **83** 1250 (2019); *Izv. Ross. Akad. Nauk Ser. Fiz.* **83** 1274 (2019)
84. Glezer A M et al. *Russ. Phys. J.* **62** 1518 (2019); *Izv. Vyssh. Uchebn. Zaved. Fiz.* (8) 196 (2019)
85. Shurygina N A et al. *Bull. Russ. Acad. Sci. Phys.* **82** (9) 37 (2018); *Izv. Ross. Akad. Nauk Ser. Fiz.* **82** (9) 50 (2018)
86. Nazarov A A, Murzaev R T *Comput. Mater. Sci.* **151** 204 (2018)
87. Nazarov A A *Lett. Mater.* **8** (3) 372 (2018); *Pis'ma Mater.* **8** (3) 372 (2018)
88. Baretzky B et al. *Rev. Adv. Mater. Sci.* **9** 45 (2005)
89. Edalati K, Horita Z *Mater Sci. Eng. A* **652** 325 (2016)
90. Razumov I K et al. *Phys. Usp.* **63** 733 (2020); *Usp. Fiz. Nauk* **190** 785 (2020)
91. Kondratyev V V, Kesarev A G, Lomaev I L *Diff. Found.* **5** 129 (2015)
92. Indenbom V L *JETP Lett.* **12** 369 (1970); *Pis'ma Zh. Eksp. Teor. Fiz.* **12** 526 (1970)
93. Ermakov A E et al. *Phys. Met. Metallogr.* **88** 211 (1999); *Fiz. Met. Metalloved.* **88** (3) 5 (1999)
94. Eckert J et al. *J. Appl. Phys.* **73** 2794 (1993)
95. Razumov I K, Gornostyrev Y N, Ermakov A E *Phys. Solid State* **61** 214 (2019); *Fiz. Tverd. Tela* **61** 346 (2019)
96. Levitas V I *Int. J. Plastic.* **106** 164 (2018)
97. Martin G *Phys. Rev. B* **30** 1424 (1984)
98. Straumal B B et al. *JETP Lett.* **112** 37 (2020); *Pis'ma Zh. Eksp. Teor. Fiz.* **112** 45 (2020)
99. Mazilkin A A et al. *Mater. Trans.* **60** 1489 (2019)
100. Prigogine I *Introduction to Thermodynamics of Irreversible Processes* (Springfield, IL: Thomas, 1955); Translated into Russian: *Vvedenie v Termodinamiku Neobratimykh Protsessov* (Moscow–Izhevsk: RKhD, 2001)
101. Kwon Y S et al. *Phys. Rev. B* **75** 144112 (2007)
102. Edalati K et al. *Mater. Sci. Eng. A* **714** 167 (2018)
103. Koneva N A, Kozlov E V, Trishkina L I *Metallofizika* **10** 49 (1991)
104. Edalati K et al. *Mater. Sci. Eng. A* **528** 7301 (2011)
105. Pereira P H R et al. *Mater. Sci. Eng. A* **593** 185 (2014)
106. Sagaradze V V et al. *Mater. Lett.* **172** 207 (2016)
107. Glezer A M, Zaichenko S G, Plotnikova M R *Bull. Russ. Acad. Sci. Phys.* **76** (1) 54 (2012); *Izv. Ross. Akad. Nauk Ser. Fiz.* **76** (1) 63 (2012)
108. Honeycombe R W K *The Plastic Deformation of Metals* (London: Edward Arnold, 1968); Translated into Russian: *Plasticheskaya Deformatsiya Metallov* (Moscow: Mir, 1972)
109. Koneva N A et al. *Mater. Sci. Eng. A* **234–236** 614 (1997)
110. Firstov S A et al. *Russ. Phys. J.* **45** 251 (2002); *Izv. Vyssh. Uchebn. Zaved. Fiz.* (3) 41 (2002)
111. Glezer A M, Pozdnyakov V A *Dokl. Phys.* **49** 570 (2004); *Dokl. Ross. Akad. Nauk* **398** 756 (2004)
112. Bykov V M, Likhachev V A, Nikonov Yu A *Fiz. Met. Metalloved.* **45** (1) 163 (1978)
113. Metlov L S *Stokhasticheskie i Termodinamicheskie Metody v Fizike* (Stochastic and Thermodynamic Methods in Physics) (Donetsk: DonNU, 2014)
114. Glezer A M, Sundeev R V, Shalimova A V *Dokl. Phys.* **56** 476 (2011); *Dokl. Ross. Akad. Nauk* **440** (1) 39 (2011)
115. El-Eskanarany M et al. *Acta Metal.* **50** 1113 (2002)
116. Tat'yanin E V et al. *Phys. Solid State* **39** 1097 (1997); *Fiz. Tverd. Tela* **39** 1237 (1997)
117. Prokoshkin S D et al. *Acta Mater.* **53** 2703 (2005)
118. Zeldovich V I et al. *Phys. Met. Metallogr.* **99** 425 (2005); *Fiz. Met. Metalloved.* **99** 90 (2005)
119. Gunderov D V *Elektron. Zh. Issled. Rossii* 1404 (2006) http://zhurnal.ape.relarn.ru/articles/2006/151.pdf
120. Pushin V G et al. *Phys. Met. Metallogr.* **83** (6) 673 (1997); *Fiz. Met. Metalloved.* **83** (6) 149 (1997)
121. Nosova G I et al. *Crystallogr. Rep.* **54** 1065 (2009); *Kristallografiya* **54** (6) 149 (2009)
122. Glezer A M et al. *Bull. Russ. Acad. Sci. Phys.* **74** 1488 (2010); *Izv. Ross. Akad. Nauk Ser. Fiz.* **74** 1576 (2010)
123. Sundeev R V et al. *Mater. Lett.* **214** 115 (2018)
124. Babanov Y A et al. *Phys. Status Solidi B* **105** 747 (1981)
125. Ershov N V et al. *Phys. Status Solidi B* **108** 103 (1981)
126. Sundeev R V et al. *Mater. Sci. Eng. A* **679** 1 (2017)
127. Perepezko J H, Hebert R J *JOM* **54** 34 (2002)
128. Shabashov V A et al. *Phys. Met. Metallogr.* **113** 489 (2012); *Fiz. Met. Metalloved.* **113** 517 (2012)
129. Sundeev R V et al. *Mater. Design* **135** 77 (2017)
130. Sagaradze V V et al. *Philos. Mag.* **96** 1724 (2016)
131. Straumal B B et al. *Acta Mater.* **122** 60 (2017)
132. Greer A L, Cheng Y Q, Ma E *Mater. Sci. Eng. R* **74** 71 (2013)
133. Langer J S *Phys. Rev. E* **77** 021502 (2008)
134. Bouchbinder E, Langer J S *Phys. Rev. Lett.* **106** 148301 (2011)
135. Khaimovich P A *Voprosy Atom. Nauki Tekh. Ser. Fiz. Radiats. Povrezh. Radiats. Materialoved.* (4) 28 (2006)
136. Chen H et al. *Nature* **367** 541 (1994)
137. Glezer A M et al. *Bull. Russ. Acad. Sci. Phys.* **73** 1233 (2009); *Izv. Ross. Akad. Nauk Ser. Fiz.* **73** 1302 (2009)
138. Sundeev R V et al. *Russ. Metallurgy* (*Metally*) **2014** (10) 778 (2014); Translated from Russian: *Deformatsiya Razrushenie Mater.* (5) 2 (2013)
139. Li J G et al. *Rev. Adv. Mater. Sci.* **18** 577 (2008)
140. Lewandowski J J, Greer A L *Nat. Mater.* **5** 15 (2006)
141. Bazlov A I et al. *Met. Mater. Int.* **24** 481 (2018)
142. Pan J et al. *Acta Mater.* **59** 5146 (2011)
143. Maaß R et al. *Appl. Phys. Lett.* **105** 171902 (2014)

144. Donovan P E, Stobbs W M *Acta Met.* **29** 1419 (1981)
145. Glezer A M et al. *Bull. Russ. Acad. Sci. Phys.* **77** 1391 (2013); *Izv. Ross. Akad. Nauk Ser. Fiz.* **77** 1687 (2013)
146. Glezer A M, Potekaev A I, Cheretaeva A O *Thermal and Time Stability of Amorphous Alloys* (Boca Raton, FL: Taylor and Francis, 2017); Translated from Russian: *Temperaturno-vremennaya Stabil'nost' Amorfnykh Splavov* (Moscow: Fizmatlit, 2016)
147. Ubyivovk E V, Boltynjuk E V, Gunderov D V *Mater. Lett.* **209** 327 (2017)
148. Aronin A et al. *J. Alloys Comp.* **715** 176 (2017)
149. Shabashov V A et al. *Philos. Mag.* 1412586 (2017)
150. Sundeev R V et al. *J. Alloys Comp.* **797** 622 (2019)
151. Feltz A *Amorphous Inorganic Materials and Glasses* (Weinheim: VCH, 1993)
152. Brazhkin V V *Phys. Usp.* **62** 623 (2019); *Usp. Fiz. Nauk* **189** 665 (2019)
153. Ponyatovsky E G et al. *JETP Lett.* **61** 222 (1995); *Pis'ma Zh. Eksp. Teor. Fiz.* **61** 217 (1995)
154. Popova S V, Brazhkin V V, Dyuzheva T I *Phys. Usp.* **51** 1064 (2008); *Usp. Fiz. Nauk* **178** 1104 (2008)
155. Glezer A M et al. *JETP Lett.* **105** 332 (2017); *Pis'ma Zh. Eksp. Teor. Fiz.* **105** 311 (2017)
156. Nakayma H, Tsuchiya K K, Umemoto M *Scr. Mater.* **44** 1781 (2001)
157. Huang Y et al. *Philos. Mag. Lett.* **84** 183 (2004)
158. Tatyanin Y V et al. *Phys. Status Solidi A* **121** 455 (1990)
159. Inaekyan K et al. *J. Alloys Comp.* **473** 71 (2009)
160. Sundeev R V, Glezer A M, Shalimova A V *J. Alloys Comp.* **611** 292 (2014)
161. Lu J P, Liu C T *Acta Mater.* **50** 3501 (2002)
162. Sundeev R V, Glezer A M, Shalimova A V *Mater. Lett.* **175** 72 (2016)
163. Korzhikov A V, Tyumentsev A N, Ditenberg I A *Phys. Met. Metallogr.* **106** 418 (2008); *Fiz. Met. Metalloved.* **106** 433 (2008)
164. Gryaznov V G, Kaprelov A M, Romanov A E *Scr. Metal.* **23** 1443 (1989)
165. Glezer A, Pozdnyakov V *Nanostruct. Mater.* **6** 767 (1995)
166. Meyers M A, Mishra A, Benson D J *Prog. Mater. Sci.* **51** 427 (2006)
167. Ovid'ko I A, Valiev R Z, Zhu Y T *Prog. Mater. Sci.* **94** 462 (2018)
168. Van Swygenhoven H, Caro A *Phys. Rev. B* **58** 11246 (1998)
169. Jarmakani H N et al. *Acta Mater.* **56** 5584 (2008)
170. Glezer A M et al. *Tech. Phys. Lett.* **42** 51 (2016); *Pis'ma Zh. Tekh. Fiz.* **42** (1) 103 (2016)
171. Ivanisenko Y et al. *Int. J. Mater. Res.* **99** 36 (2008)
172. Shurygina N A et al. *Mater. Sci. Eng. IOP Conf. Ser.* **709** 044090 (2020)
173. Zhang Q S et al. *Acta Mater.* **58** 904 (2010)
174. Gunderov D, Astanin V *Metals* **10** 415 (2020)
175. Rosner H et al. *Ultramicroscopy* **142** 1 (2014)
176. Abrosimova A et al. *Mater. Lett.* **252** 114 (2019)
177. Louzguine-Luzgin D V et al. *J. Non-Cryst. Solids* **396–397** 20 (2014)
178. Glezer A M et al. *Mater. Lett.* **281** 128659 (2020)
179. Mazilkin A et al. *Mater. Trans.* **60** 1489 (2019)
180. Hriplivets I A et al. *Bull. Russ. Acad. Sci. Phys.* **85** 782 (2021); *Izv. Ross. Akad. Nauk Ser. Fiz.* **85** 1008 (2021)
181. Glezer A M et al. *Dokl. Akad. Nauk SSSR* **272** 1114 (1983)
182. Startsev V I, Il'ichev V Ya, Pustovalov V V *Plastichnost' i Prochnost' Metallov i Splavov pri Nizkikh Temperaturakh* (Plasticity and Strength of Metals and Alloys at Low Temperatures) (Moscow: Metallurgiya, 1975)
183. Mironchuk B et al. *Mater. Lett.* **273** 126631 (2020)
184. Boltynjuk E et al. *Defect Diff. Forum* **385** 319 (2018)
185. Beygelzimer Y *Mech. Mater.* **37** 753 (2005)
186. Glezer A M, Tomchuk A A, Rassadina T V *Russ. Metallurgy* (*Metally*) **2015** (4) 295 (2015); Translated from Russian: *Deformatsiya Razrushenie Mater.* (4) 15 (2014)
187. Beygelzimer Y *Mater. Sci. Forum* **683** 213 (2011)
188. Korneva A et al. *Mater. Charact.* **1144** 151 (2016)
189. Edalati K et al. *Mater. Res. Lett.* **10** 163 (2022)
190. Sauvage X et al. *Scr. Mater.* **60** 1056 (2009)
191. Jang J S C, Koch C C *J. Mater. Res.* **5** 498 (1990)
192. Morri D G, Bonghalem A, in *Proc. Intern. Symp. on Metastable, Mechanically Alloyed and Nanocrystalline Materials, Grenoble, 1994*, p. 552
193. Varin R A, Bystrzycki J, Calka A *Mater. Res. Soc. Symp. Proc.* **552** 145 (1999)
194. Dadras M M, Morris D G *Scr. Mater.* **28** 1245 (1993)
195. Pochet P et al. *Phys. Rev. B* **52** 4006 (1995)
196. Rentenberger C, Karnthaler H P *Acta Metal.* **56** 2526 (2008)
197. Bekker H et al. *Mater. Sci. Forum* **88–90** 27 (1992)
198. Starenchenko V A, Pantyukhova O D, Starenchenko S V *Phys. Solid State* **44** 994 (2002); *Fiz. Tverd. Tela* **44** 950 (2002)
199. Hosokawa A et al. *Mater. Trans.* **55** 1286 (2014)
200. Glezer A M et al. *J. Alloys Comp.* **744** 791 (2018)
201. Marcinkowski M J et al. *J. Mater. Sci.* **10** 406 (1975)
202. Straumal B B et al. *Diffus. Found.* **5** 95 (2015)
203. Swann P R, Duff W R, Fisher R M *Metal. Trans.* **3** 409 (1972)
204. Glezer A M et al. *J. Alloys Comp.* **866** 159021 (2021)
205. Inden G *Z. Metallkunde* **68** 529 (1977)
206. Iijima Y, Lee C-G *Acta Met. Mater.* **43** 1183 (1995)
207. Tokei Z, Bernardini J, Beke D L *Acta Mater.* **47** 1371 (1999)
208. Kakehashi Y *Modern Theory of Magnetism in Metals and Alloys* (Springer Series in Solid-State Sciences, Vol. 175) (Berlin: Springer, 2012)
209. Sundeev R V et al. *Mater. Lett.* **331** 133513 (2023)
210. Bellon P, Averback R S *Phys. Rev. Lett.* **74** 1819 (1995)
211. Gleiter H *Acta Metal.* **16** 455 (1968)
212. Hernández-Escobar D, Kawasaki M, Boehlert C J *Int. Mater. Rev.* **67** (3) 231 (2022)
213. Ekiz E H et al. *Acta Mater.* **72** 178 (2014)
214. Permyakova I E et al. *Russ. Phys. J.* **61** 428 (2018); *Izv. Vyssh. Uchebn. Zaved. Fiz.* (3) 28 (2018)
215. Danilenko V N et al. *Mater. Lett.* **236** 51 (2019)
216. Bazarnik P et al. *Mater. Sci. Eng. A* **833** 142549 (2022)
217. Permyakova I E et al. *JETP Lett.* **113** 471 (2021); *Pis'ma Zh. Eksp. Teor. Fiz.* **113** 468 (2021)